Combined linear regression and Monte Carlo approach to modelling exposure age depth profiles

Yiran Wang[1, 2], Michael E. Oskin[1]

[1]Department of Earth and Planetary Sciences, UC Davis, Davis, 95616, USA
[2]Earth Observatory of Singapore, Nanyang Technological University, 639798, Singapore

Correspondence to: Yiran Wang (yrwwang@ucdavis.edu)

Abstract. We introduce a set of methods for analyzing cosmogenic-nuclide depth profiles that formally integrates ~~surface erosion~~denudation and muogenic production, while retaining the advantages of ~~the~~ linear inversion. For surfaces with ~~erosion~~denudation, we present solutions for both ~~erosion~~denudation rate and total ~~eroded thickness~~denudation depth, each with their own advantages. ~~For practical applications, erosion must be constrained from external information, such as soil-profile analysis.~~ By combining linear inversion with Monte Carlo simulation of error propagation, our method jointly assesses uncertainty arising from measurement error and ~~erosion~~denudation constraints. Using simulated depth profiles and natural-example depth profile data sets from the Beida River, northwest China and Lees Ferry, Arizona, we show that our methods robustly produce ~~comparable ages for surfaces with different erosion rates~~ accurate age and inheritance. ~~Through hypothetical examples, we further show that both the erosion rate and eroded-thickness approaches~~ estimations for surfaces under varying circumstances. The denudation-depth approach can theoretically produce ~~reasonable~~reasonably accurate age estimates ~~so long as the~~ even when total ~~erosion less than twice~~denudation reaches five-times the nucleon attenuation length. ~~Overall~~The denudation-rate approach, on the other hand, has the advantage of allowing direct exploration of trade-offs between exposure age and denudation rate. Out of all the factors, lack of precise constraints for ~~erosion~~denudation rate or depth tends to be the largest contributor of age uncertainty, ~~compared to the~~while negligible error results from ~~omitting~~our approximation of muogenic production ~~or radioactive decay~~.using the denudation-depth approach.

1 Introduction

In-situ terrestrial cosmogenic nuclide (~~CN~~TCN) dating, especially with ^{10}Be, is a widely applied tool to estimate landform ages (e.g., Granger et al., 2013). These dates are affected by landscape processes that either remove or add ~~CNs~~TCNs, lending uncertainty that may be difficult to assess without additional information. Ages of landforms constructed from sediments, such as a stream terrace, may be affected by ~~CNs~~TCNs acquired by the sediments prior to deposition, termed inheritance, leading to erroneously older dates (Brocard et al., 2003; Hancock et al., 1999; Repka et al., 1997). Conversely, even a low rate of ~~erosion~~denudation of a landform after its formation will bias surface-exposure ages younger (Lal, 1991). Under the condition of no ~~erosion, the~~ denudation, solving a depth-profile ~~approach,~~ of TCN concentrations via linear inversion – a technique first

developed by Anderson et al. (1996~~),~~) – provides a robust ~~technique~~approach for estimating surface age and inheritance from a landform comprised of sediments. ~~The effect of erosion~~However, this method suffers from the deficit of not incorporating denudation or muogenic production process, and has been succeeded by forward-modelling approaches (e.g. Hidy et al., 2010). Despite its deficits, however, ~~is difficult~~linear regression retains advantages as a robust and straightforward approach to ~~discern from a~~invert for exposure age. Herein we revisit the application of linear regression for TCN depth ~~profile of CN concentrations, leading to a trade-off between model age and erosion rate. Though it is theoretically possible to solve for erosion rate~~profiles with ~~sufficient number, precision, and depth of sampling (Brocard et al., 2003), realistic sampling scenarios require external constraints~~an updated approach, building upon the simplicity of ~~erosion to fully assess a landform~~the original technique, but expanding its application to surfaces with independently constrained denudation histories, and increasing the accuracy of the age~~.~~ and inheritance results by taking muogenic production into account.

~~There are generally two groups of approaches from which the surface exposure age can be estimated from a CN depth profile. The first group relies on linear inversion of the relationship between concentration and nucleogenic production rate at depth (i.e., Anderson et al., 1996). This approach, as originally formulated, accounts for nucleon (neutron and proton) spallation production of CNs that make up ~98% of surface production and decreases sharply within the upper two meters of sediment. Muons, accounting for the other 2% of surface production, penetrate much deeper than nucleons (Braucher et al., 2003; Heisinger et al., 2002b, 2002a), such that muogenic production barely decreases within the upper two meters of a depth profile and therefore may be ignored, to first order (Figure 1a). This inversion approach has the advantage of being straightforward to apply to determine an exposure age without any prior knowledge. However, currently applied linear inversion techniques do not fully account for measurement uncertainty in model ages, and also do not explicitly account for the effects of erosion. In addition, ignoring muogenic production could lead to minor overestimation of surface age and significant overestimation of inheritance, especially for surfaces undergoing erosion. The second group of approaches uses forward modelling to find best-fit depth-concentration curves, such as with χ^2 minimization (e.g. Braucher et al., 2009; Hidy et al., 2010; Matsushi et al., 2006; Riihimaki et al., 2006), or Bayesian inference (e.g. Laloy et al., 2017; Marrero et al., 2016). These approaches have the advantage of accounting for muogenic production and can include erosion into the inversion process. However, the accuracy and efficiency of these approaches largely rely on researchers' prior knowledge of the surface age and inheritance.~~

~~In this paper, we present a combined linear regression and Monte-Carlo approach to analyzing ^{10}Be depth profiles that formally integrates surface erosion and muogenic production into exposure age modelling. This approach builds upon the simplicity and minimum prior knowledge needed for the linear regression approach, but expands its application to surfaces with independently constrained erosion histories and increases the accuracy of the age and inheritance results by taking muogenic production into account. To demonstrate application of this approach, we examine an example sample site from our previously published~~As an inverse approach, our least-squares linear regression directly solves for a best-fit age and inheritance, while treating the denudation rate or denudation depth as a model input, rather than an output of the model. It may be used with Monte Carlo sampling to explore the full distribution of possible ages and inheritance from the variation of input parameters. As an inverse approach, linear regression returns a best estimate without requiring extensive calculations and repetitions. This

is useful to derive an exposure age directly, or as a starting point for forward models (e.g. Hidy et al., 2010; Laloy et al., 2017; Marrero et al., 2016). In the latter case, linear inversion may help researchers tune the boundary values for the forward models to get better simulation results.

In this paper, we present a general inversion which incorporates muogenic process, and two derivative approaches for age inversion at sites with constant denudation rate. The first derivative approach directly applies a constant denudation rate but requires simplification by omitting muogenic production. This approach provides a useful tool to explore the trade-offs between denudation rate and exposure age but introduces systematic errors as denudation rate increases due to the exclusion of muogenic production. The second derivative approach introduces a solution for a constant denudation depth with a Taylor-series approximation for the muogenic production terms. With this approximation, linear regression produces robust age estimates even for surfaces with a large amount of denudation. To show the application of these techniques, we present applications to pseudo-realistic depth profiles under various scenarios. We also apply our approach to two previously published example sample sites, one from the Beida River in western China from our own work (Wang et al., 2020), and ~~we re-analyze~~ one from the Lees Ferry ~~stream terrace~~ site ~~example~~on the Colorado River from Hidy et al. (2010~~)~~), to ~~compare~~demonstrate model performance for realistic cases. These examples show that our ~~method with their Monte-Carlo χ^2 minimization~~revised linear-regression approach~~. We also discuss the trade-off of surface erosion with~~ is robust and can be applied to most exposure ~~age estimation, the impact of muons and radioactive decay on age and inheritance calculations~~dating scenarios.

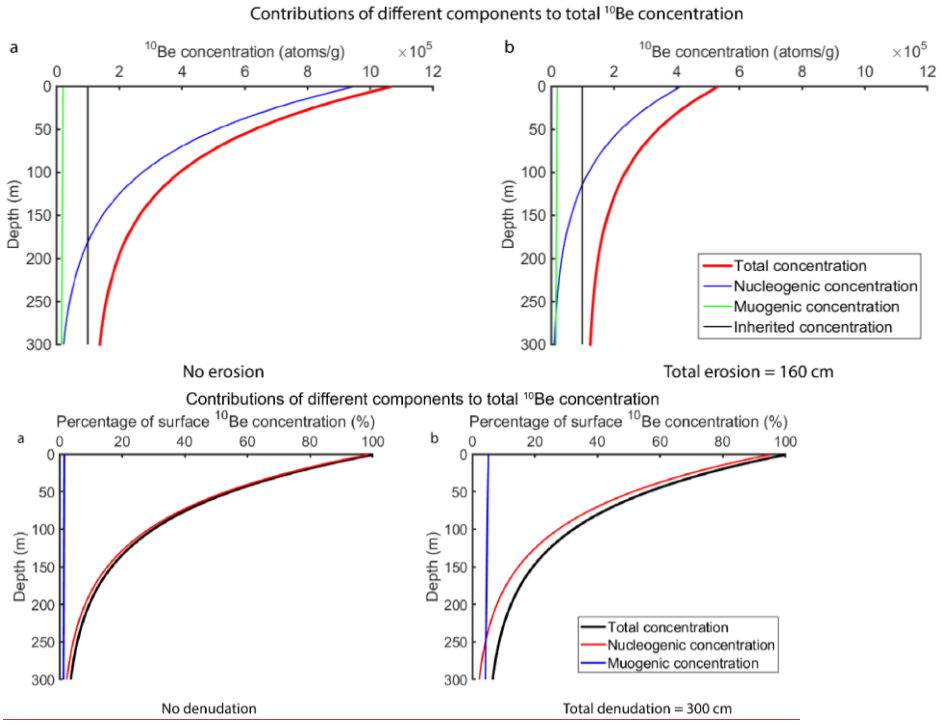

Figure 1 Depth-concentration profiles with different contributing components for a hypothetical surface. ~~All conditions~~The profiles are ~~the same for both figures: total surface~~calculated based on a sea level high latitude production rate~~, 10 atoms/(g*yr); sediment density, 2g/cm3; the relative contributions of nucleons and muons (negative and fast) to the total~~ ^{10}Be (nucleogenic production ~~are 97.85%, 1.5% and~~rate of 4.11 atoms/g, Martin et al., 2017; muogenic production rate of 0.~~65%, with Λ equal to 160 0735 atoms/g/cm^2, 1500 g/cm^2 and 5300 g/cm^2, respectively ((Braucher et al., 2003)~~Balco, 2017)~~).~~. All the concentrations are normalized to a~~. percentage of the total surface concentration. a.~~ Surface with ~~zero erosion.~~no denudation. b. Surface with steady ~~erosion, eroded thickness~~denudation rate; denudation depth equal to ~~two attenuation length (160~~300 cm~~).~~.

2 Methods

2.1 General inversion

Under conditions of constant production rate and constant ~~erosion~~denudation rate, a surface that was exposed at time t would have a concentration of a cosmogenic nuclide (N_z) as (Balco et al., 2008; Braucher et al., 2009; Lal, 1991; Lal and Arnold, 1985):

$$N_z(t) = P_{n,0}e^{-\frac{\rho z}{\Lambda_n}}\left(\frac{1-e^{-\left(\frac{\rho r}{\Lambda_n}+\lambda\right)t}}{\frac{\rho r}{\Lambda_n}+\lambda}\right)\left(\frac{1-e^{-\left(\frac{\rho \varepsilon}{\Lambda_n}+\lambda\right)t}}{\frac{\rho \varepsilon}{\Lambda_n}+\lambda}\right) + P_{m_1,0}e^{-\frac{\rho z}{\Lambda_{m1}}}\left(\frac{1-e^{-\left(\frac{\rho r}{\Lambda_{m1}}+\lambda\right)t}}{\frac{\rho r}{\Lambda_{m1}}+\lambda}\right)\left(\frac{1-e^{-\left(\frac{\rho \varepsilon}{\Lambda_{m1}}+\lambda\right)t}}{\frac{\rho \varepsilon}{\Lambda_{m1}}+\lambda}\right) +$$

$$P_{m_2,0}e^{-\frac{\rho z}{\Lambda_{m2}}}\left(\frac{1-e^{-\left(\frac{\rho r}{\Lambda_{m2}}+\lambda\right)t}e^{-\left(\frac{\rho \varepsilon}{\Lambda_{m2}}+\lambda\right)t}}{\frac{\rho r}{\Lambda_{m2}}\frac{\rho \varepsilon}{\Lambda_{m2}}+\lambda}\right) \quad (1)$$

where $P_{n,0}$, $P_{m_1,0}$, and $P_{m_2,0}$ are the surface production rate induced by nucleons, negative muons, and fast muons; $\Lambda_n, \Lambda_{m1}, and\ \Lambda_{m2}$ are the attenuation scale lengths (g/cm^2) of the nucleons and muons (negative and fast), respectively; z is the depth beneath the target surface; λ is the decay constant, and ~~r~~ε is a constant ~~erosion~~denudation rate, if applicable. For our purposes, we model ages using ^{10}Be, with a half-life of 1.39 Myr (Chmeleff et al., 2010; Korschinek et al., 2010~~; Nishiizumi et al., 2007~~), due to its wide applicability to quartz-bearing sediments (Cockburn and Summerfield, 2004; Granger et al., 2013; Rixhon et al., 2017).

Based on eq. 1, the production of cosmogenic nuclides may be simplified into two major components: the production rate at specific depth (P_z), and the effective exposure age of the site (T_e), which is the time that is required to accumulate concentration N_z at production rate P_z without erosion and radioactive decay. Therefore eq. 1 may be rearranged into:

$$N_z(t) = \sum_i P_{zi}T_{ei} \quad (2a)$$

$$\text{where } P_{zi} = P_{i,0}e^{-\frac{\rho z}{\Lambda_i}}, T_{ei} = \left(\frac{1-e^{-\left(\frac{\rho r}{\Lambda_i}+\lambda\right)t}}{\frac{\rho r}{\Lambda_i}+\lambda}\right)\left(\frac{1-e^{-\left(\frac{\rho \varepsilon}{\Lambda_i}+\lambda\right)t}}{\frac{\rho \varepsilon}{\Lambda_i}+\lambda}\right), i = n, m_1, m_2 \quad (2b)$$

The ^{10}Be concentration measured from a suite of samples (~~Figure~~Fig. 1), C, has two components: the in-situ produced concentration, N_z, and the inherited concentration, C_{inh},

$$C = \sum_i P_{zi}T_{ei} + C_{inh}. \quad (3)$$

Though ^{10}Be concentration (C) is exponential to the burial depth, based on equation 2 and 3, when there is no ~~surface erosion~~ (~~r~~denudation ($\varepsilon \approx 0$), $T_{en} = T_{em1} = T_{em2}$, and therefore eq. 3 can be rearranged as:

$$C = T_e \sum_i P_{zi} + C_{inh}. \quad (4a)$$

$$\text{where } T_e = \left(\frac{1-e^{-\lambda t}}{\lambda}\right) \quad (4b)$$

This equation is an update to the linear regression approach first proposed by Anderson et al. (1996) that accounts for both nucleon and muon production, as well as radioactive decay. For the case of no ~~erosion, CN~~denudation, TCN concentration is linear to the sum of production rates via all pathways ($\sum_i P_{zi}$), and T_e and C_{inh} are the slope and intercept of this linear relationship respectively. Therefore, similar to the approach proposed by Anderson et al. (1996), we can apply ~~linear~~ least-squares linear regression to find the slope (T_e) and intercept (C_{inh}) of the best fit line to the concentration vs. production rate data of the depth profile. The exposure age, factoring in decay, may be calculated directly by rearranging eq. 4b:

$$t = -\frac{\ln(1-T_e\lambda)}{\lambda} \quad (5)$$

2.2 Inversion with ~~erosion~~denudation rate

For sites with constant ~~erosion~~denudation rate, ~~ε~~, the effective age for each pathway (nucleons or muons) would be different, due to their different attenuation lengths. But an approximation may be made by omitting the muogenic production, on the basis that muogenic production only makes up ~~~2%~~a very small fraction of the total surface production (Braucher et al., 2003, 2011, 2013; Heisinger et al., 2002b, 2002a; Balco 2008, 2017), and eq. 3 may be further simplified to

$$C = P_{zn}T_{en} + C_{inh}, \qquad (6)$$

Using eq. 6, a linear Least-Squares regression can be applied to find the best-fit T_{en} and C_{inh}, which leads to the estimated exposure age

$$t = -\frac{\ln(1-T_{en}B)}{B} \quad (7a) \qquad \text{where } B = \frac{\rho\varepsilon}{\Lambda_n} + \lambda \quad (7b)$$

This solution illustrates the utility of separating the age model for finding T_{en} from the effect of ~~erosion~~denudation rate, contained within the parameter *B*. ~~Considering only nucleons, there is no information from a depth profile of CN concentrations that constrains erosion~~Though the error introduced to omitting muogenic production grows as the denudation rate~~, except for the upper limit of~~ increases, this ~~rate that yields an infinite~~approach (eq. 7) provides a useful tool to examine the relationship between exposure age ~~when B = 1/T$_{en}$~~and denudation rate.

2.3 Inversion with ~~eroded thickness~~denudation depth

For many practical cases, it may be more straightforward to estimate total ~~eroded thickness~~denudation depth (D) from field evidence such as through soil-profile analysis, rather than ~~an erosion~~a denudation rate~~.~~ (e.g. Ebert et al., 2012; Hidy et al, 2010; Ruszkiczay-Rüdiger et al., 2016). With ~~eroded thickness~~denudation depth, the effective age of each pathway may be rewritten as

$$T_{ei} = \left(\frac{1-e^{-\left(\frac{\rho D}{\Lambda_i}+\lambda t\right)}}{\frac{\rho D}{\Lambda_i t}+\lambda}\right), i = n, m_1, m_2 \qquad (8)$$

Here we explore the application of this equation with the inclusion of muogenic production. Using a series expansion, we rewrite the effective age related to muons~~,~~ (negative and fast), T_{em}, into a fraction, g, of the effective age related to nucleons, T_{en}. The fraction g can be approximated solely from knowledge of the ~~eroded thickness~~denudation depth, D (see Appendix for derivation):

$$g_i = \frac{T_{emi}}{T_{en}} \approx e^{-\frac{1}{2}\left(\frac{\rho D}{\Lambda_{mi}}-\frac{\rho D}{\Lambda_n}\right)+\frac{1}{24}\left[\left(\frac{\rho D}{\Lambda_{mi}}\right)^2-\left(\frac{\rho D}{\Lambda_n}\right)^2\right]}, i = 1, 2 \qquad (9)$$

Bringing g_i into eq. 3, we have

$$C(z) = P_{zn}T_{en} + P_{zm_1}g_1T_{en} + P_{zm_2}g_2T_{en} + C_{inh} = P_{ze}T_{en} + C_{inh},$$

$$P_{ze} = \left(P_{zn} + P_{zm_1}g_1 + P_{zm_2}g_2\right) \qquad (10)$$

where P_{ze} is the effective production rate from both nucleons and muons under the condition of a finite amount of ~~erosion over the lifetime of the deposit. Note that the robustness of the muogenic production approximation (see Appendix) illustrates how erosion depth (or rate) may not be well constrained from concentration-depth profiles alone, even when including muogenic production, and even though a unique solution for age, inheritance, and erosion rate formally exists (Broccard et al., 2003).~~steady denudation over the lifetime of the deposit.

Using equation 10, T_{en} and C_{inh} can be found by applying least-squares linear regression with known production rates, ~~eroded thickness~~denudation, and sample concentrations, similar to the general inversion case for no ~~erosion~~denudation described by equation 4.

To estimate the exposure age, we need to find the solution for

$$f(t) = \left(\frac{1 - e^{-\left(\frac{\rho D}{t\Lambda_n} + \lambda\right)t}}{\frac{\rho D}{t\Lambda_n} + \lambda} \right) - T_{en} = 0 \quad (11)$$

While the complicated form of eq. 11 prohibits a direct solution, t may be found iteratively by applying the Newton's method. Using the derivative of eq. 11,

$$f'(t) = -\lambda e^{-\left(\frac{\rho D}{\Lambda_n}\right)D - \lambda t} - \frac{\rho D T_{en}}{\Lambda_n t^2}, \quad (12)$$

the exposure age can then be iterated from

$$t_{n+1} = t_n - \frac{f(t_n)}{f'(t_n)} \quad (13)$$

with initial guess, $t_0 = T_{en}$.

3 Applications~~2.4 Uncertainty treatment with Monte Carlo simulation~~

~~**In our model (https://github.com/YiranWangYR/10BeLeastSquares), we**~~

We present a set of example applications of linear regression to TCN depth profiles using both the denudation-rate (eqs. 6, 7) and the denudation-depth technique (eqs. 8-13). We begin with simulated TCN depth profiles to explore the impacts of scatter of sample concentration, low inheritance, denudation, and sample depth on the accuracy and precision of our approach, and to compare the performance of linear regression with the estimations using a Bayesian Monte-Carlo Markov Chain approach. We then demonstrate the linear regression technique with two case examples. For the Beida River T2 terrace of the North Qilian Shan, China (Wang et al., 2020), we demonstrate using the denudation-rate approach to explore the possible range of exposure age and the trade-offs between age and denudation rate; we also demonstrate how to use the denudation-depth approach combined with Monte Carlo simulation to estimate the full distribution of exposure age and inheritance. For the Lees Ferry site on the Colorado River (Hidy et al., 2010), we compare results from our denudation-depth approach with the originally published data.

To explore the full distribution of possible estimated age and inheritance, we consider the uncertainty ~~of the exposure age~~ propagated from ~~four~~five different sources: ~~analytical uncertainties~~uncertainty of the ^{10}Be concentration measurements, uncertainty of sample depths, uncertainty of ~~the erosion~~sediment density, uncertainty of the denudation depth or rate, and the uncertainties related to ~~CN~~TCN production and decay (i.e., the attenuation length, production rates, etc.). These uncertainties propagate sequentially, first from ^{10}Be concentration ~~and~~, sample depths, and sediment density through the least-squares linear regression process, and second from ~~erosion~~denudation rate or depth through converting exposure age from the effective exposure age (Te). ~~The uncertainties related to ^{10}Be production and decay affect both steps.~~

Because of the limited sample sizes typical of most studies, and the variance in both concentration and depth, we ~~propose a Monte Carlo simulation approach to determine the range of exposure age and inheritance. For each iteration, we randomly select a group of values (C, z, P_z, and r or D, etc.) from their corresponding probability density functions. The slope and intercept (T_e and C_{inh}) are found via least-squares linear regression of the concentration versus production rate as a function of depth. Then the exposure age, t, may be calculated using eq. 5, eq. 8, or eq. 11 through 13. Repeating these steps yields a distribution representing the probability of t and C_{inh} of the samples. By increasing the number of iterations, the shape of the resulting probability distribution becomes apparent and the accuracy increases~~apply a Monte Carlo sampling approach for the range of each input parameter. The code used here is archived in Github (https://github.com/YiranWangYR/10BeLeastSquares). Our procedure includes the following steps. Step 1: generate all the input parameters for one model, sampling distributions for ^{10}Be concentration, sample depth, denudation rate/depth, production rate, attenuation length, etc. Depending on the parameter, we represent uncertainty as either a normal or uniform distribution. Step 2: fit these sampled input parameters with eq. 4 or eq. 6 or eq. 10 to derive best-fit sample T_{en} and inheritance values. Step 3: calculate the exposure age use T_{en} from step 2 and parameters generated from step 1 using eq. 5 or eq. 7 or eqs. 11-13. Repeat step 1-3 for many times to produce a distribution of age and inheritance results.

3.1 Simulated TCN depth profiles

To demonstrate how our approach will perform under different circumstances, we generate a series of simulated depth profiles to test how closely the estimated age and inheritance will reflect the true values. With these profiles, four different scenarios are tested: varying degrees of random deviation of sample concentrations, varying amount of denudation, low inheritance, and deep sample depth. For comparison, we use a Bayesian Monte-Carlo Markov Chain (Metropolis–Hastings algorithm) approach (codes: https://github.com/YiranWangYR/10BeLeastSquares/blob/581892b6b50a255ab30810efbe6e6e68c0b984c5/Be10_LRvsBayesian.m) to estimate the exposure age and inheritance along with our linear regression approach. We choose to use our own coding following Bayesian inversion principles instead of a published codes because, first, we need to ensure the input variables are the same for both approaches; second, to be statistically significant, we need to apply both approaches several hundred times for each scenario, therefore manually doing so with published codes would be extremely time consuming.

For all simulated profiles, we set the true age and inheritance to be 200 kyr and 100 × 10^3 atoms/g except for the low inheritance scenario, where we set inheritance to 0 and 5000 atoms/g. Each simulated profile contains 6 samples; to mimic realistic scatter of sample concentrations, all the simulated samples are deviated from the true profile based on an assigned normal distribution of either 1, 2, 5, or 10% standard deviation. Analytical uncertainties (2% standard deviation) are assigned to each sample of the simulated profile to mimic realistic values. For each scenario, 500 simulated profiles are generated and inverted for age and inheritance using both the linear regression and Bayesian approaches. The details of our simulation process and the parameters we used for each scenario are listed in Table 1.

3 Applications

In this section, we apply our model to two published ^{10}Be depth profile sample sites. One from our own published research of the Beida River T2 terrace of the North Qilian Shan, China (Wang et al., 2020). We use this site to demonstrate the modeling steps in detail. The second site is the Lees Ferry site, an example from Hidy et al. (2010). We use this second site to compare our modeling results with their widely used X^2 minimization technique.

3.1 Beida River Example

3.1.1 Sample site

In western China, the Qilian Shan orogen serves as the northeastern margin and youngest growing portion of the Tibetan plateau. The Beida River is the largest river that flows northward across the western portion of the North Qilian Shan. At least three principal generations of fill terraces (T1, T2, and T3) are preserved along the Beida River inside the Qilian Shan mountain range. Mapping and dating of these terraces make it possible to understand the aggradation-incision process of the river and interpret the tectonic deformation of the North Qilian Shan (Wang et al., 2020). Our sample site is located on a T2 terrace tread, ~5 km upstream of the mountain front, and more than 200 m above present riverbed. The T2 terrace at this location has been dissected by gullies into several isolated lobes, suggesting that remnant terrace treads might have experienced some degree of surface erosion. Loess of ~130 cm thickness is deposited atop of the terrace tread. A OSL sample at the loess bottom suggests loess deposition started around 8.3±1.2 kyr (Wang et al., 2020).

We excavated a sample pit ~2 m deep on this T2 terrace tread. The soil profile developed on the terrace fill shows a 20 cm-thick remnant reddened B horizon with clay directly in contact with the base of the loess cover (Supplement figures of Wang et al., 2020). An unknown thickness of the B horizon, along with the original soil A horizon, are missing, and were presumably eroded prior to loess deposition. We therefore interpret that there may have been 20-60 cm of erosion of the terrace tread, before the onset of loess accumulation. We collected six samples of medium to coarse sand from up to 2 m below the base of the loess. These samples were processed at Arizona State University following standard chemical cleaning and etching procedures. AMS measurements of these samples were conducted at the Prime Lab of Purdue University. The ^{10}Be concentrations reported by the Prime Lab are listed in table 1.

Table 1 Sample information and ^{10}Be concentration of Beida River T2 site (Wang et al., 2020)Parameters used for each simulation scenario.

Scenario	1: Deviation of concentration	2: low inheritance	3: denudation	4: deep profile
Numbers of profiles	500			
True exposure age (kyr)	200			

Sample ID	Coordinates and elevation	Depth (cm, below soil bottom)	Thickness (cm)	Dissolved quartz (g)	Carrier Mass (g)	Corrected $^{10}Be/^{9}Be$	^{10}Be Production rate[1] (atoms/(g × yr))	1σ Error (atoms/g)Nucleon	10	
BT2-2-20	39.57443N, 97.99988	40	10	22.21001	1.42E-12			0.33669014	1497204	22001

	E; 2300 m Muon (negative)							
BT2-2-45	Muon (fast)	65	10	14.738835	0.34244051	6.42E-13	1035575	24187
Attenuation (g/cm^2)	Nucleon	160						
	Muon (negative)	1500						
	Muon (fast)	4320						
Decay constant(s^{-1})		4.997E-07						
Sediment density (g/cm^3)		2.0						
Concentration uncertainty[2] (1σ, %)		2						
BT2-2-75Deviation of concentration[3] (1σ, %)	75	2, 5, and 10	14.793915	0.341835	3.76E-131 and 5	602740	15467	
Sample depths (cm)		BT2-2-110[25; 50; 70; 110; 150; 200]	[25; 50; 70;	130[25; 50; 70; 110; 150; 200]	10 [325; 350;	9.02134	0.34213 1.64E-13 4303 35 16094	

					110; 150; 200]		370; 410; 450; 500]						
Sample depth uncertainty (1σ; cm)	5												
Inheritance (×10[3] atoms/g)	100				0 and 5	100	100						
~~BT2-2-150~~Denudation (cm)	0	~~160~~	~~10~~	~~2-50438~~	~~0.33589~~	~~3.13E-13~~ 1-, 2-, 3-, and 5-times attenuation length	~~3101410~~-, 2- and 5-times attenuation length						~~7535~~
~~BT2-2-180~~Eq. used for linear regression	eq. 4				eq. ~~20004~~	eq. 10	eq. ~~30.158464~~ and eq. 10	~~0.30283~~	~~3.89E-13~~	~~271258~~	~~5698~~		

[1]. Production rate is calculated based on a hypothetical middle latitude, 1000 m elevation site (Stone 2000; Braucher 2011)

[2]. The analytical uncertainty of sample concentration.

[3]. The amount that the mean sample concentration deviates from the true concentration.

3.1.1 Deviation of sample concentrations

We test three sets of simulations under different degrees of imposed deviation of sample concentrations (standard deviation of 2%, 5%, and 10%) with no denudation. The 2% deviation case matches the analytical uncertainty (2%), while the 5% and 10% cases introduce excess scatter, as is typically found in TCN depth profiles. For the case with 2% of deviation, we find both linear regression and Bayesian approaches yield results centered around the true age (200 kyr). For the linear regression approach, 95% of the mean ages fall within 4.0-4.5% error range of the true age, while for the Bayesian approach 95% of the mean age fall within 3.0-3.5% error range of the true age. The Bayesian approach works slightly better than linear regression for the more extreme (noisier) cases (Fig. 2, S1). For inheritance estimation, similar to the exposure age, both approaches return results centered around the true value (100,000 atoms/g), and a Bayesian approach again performs somewhat better for noisier data. When the sample deviation increases to 5%, then to 10%, the estimated age and inheritance values remain centered

Deleted Cells
Deleted Cells
Deleted Cells
Deleted Cells
Deleted Cells
Deleted Cells
Deleted Cells
Deleted Cells

on the correct age and inheritance while the ranges of the mean estimations for both approaches expand significantly, indicating a decrease of precision as the noise level increases (Fig. 2, fig. S1-S3). With 5% of deviation, 95% of the estimated ages fall within 10% and 8% ranges of the true value for linear regression and Bayesian approach respectively. With 10% of deviation, 95% of the estimated age fall within 21% and 17% ranges of the true value for linear regression and Bayesian approach respectively. We also find the error range for the estimation results from the linear regression is moderately larger than a Bayesian approach (Fig. S1-S3). Importantly, we find that while each approach provides different estimation results for the same set of samples, one model does not consistently perform better than the other (Fig. S1-S3). About 40-45% of the time the linear regression returns results closer to the true age than the Bayesian approach.

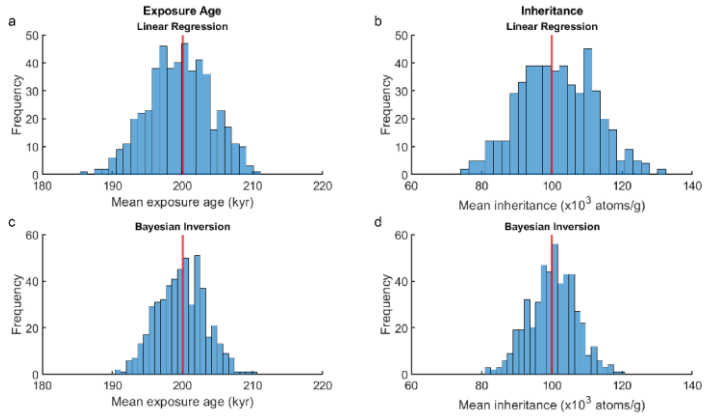

Figure 2 Distribution of mean exposure age (a and c) and inheritance (b and d) estimated from linear regression (eq. 4; a and b) and a Bayesian approach (c and d) for 500 simulated profiles with 2% of imposed sample deviation. Red vertical line annotates the true age and true inheritance.

3.1.2 Low inheritance

For profiles with very low or zero inheritance, we find that imposing the physically reasonable prerequisite that inheritance must be non-negative may lead to underestimation of the exposure age. This occurs for both linear regression and Bayesian approaches that we tested. For profiles generated with 5% imposed deviation of sample concentrations and zero inheritance (Table 1), we compare three different ways to treat negative inheritance under linear regression: permit negative inheritance during inversion, do not permit negative inheritance during inversion through setting a zero-inheritance boundary condition, and excluding negative inheritance outcomes after inversion. For the Bayesian approach, we compare boundary conditions of permitting versus not permitting negative inheritance. The distributions of the mean exposure age (Fig. 3; fig. S4) show that, for linear regression, not permitting negative inheritance leads to a skewed distribution, with the results centered around 197 kyr, while excluding negative inheritance afterwards produces a further biased result with a mean centering around 193 kyr.

The Bayesian approach also performs slightly less well; not permitting negative inheritance leads to the estimated results centering around 195 kyr. When negative inheritance is permitted during inversion process, both approaches produce results that centered well around the true age. For a more realistic case, when we set the true inheritance of the profile as 5000 atoms/g, the estimated exposure ages are also deviated to be younger (though not as much as the zero-inheritance case) unless negative inheritance is permitted during the inversion (Fig. S5).

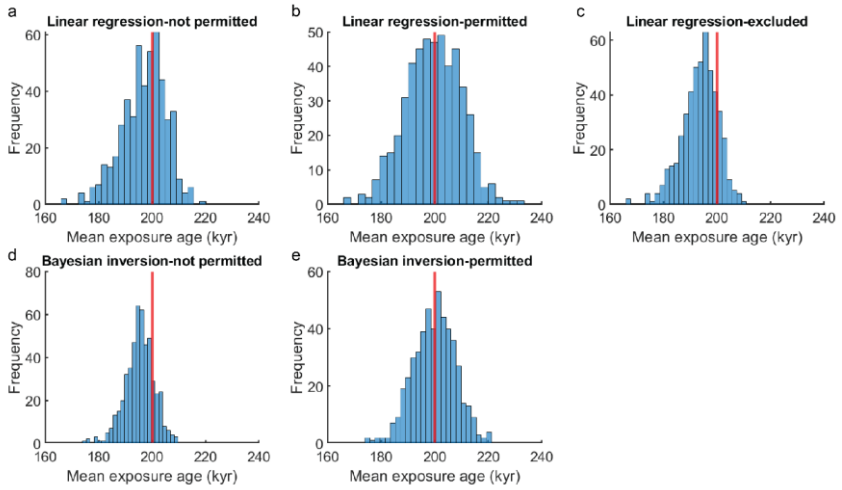

Figure 3 Distribution of mean exposure age estimated from linear regression (eq. 4; a, b, and c) and a Bayesian approach (d and e) for 500 simulated profiles with 0 inheritance and 5% of imposed sample deviation. a and d, not permitting negative inheritance during inversion. b and e, permit negative inheritance during inversion, c, excluding negative inheritance results after inversion. Red vertical line annotates the true age and true inheritance.

3.1.3 Denudation depth

To test the robustness of our denudation-depth approach, we tested simulated TCN depth profiles with total denudation of 1, 2, 3, and 5-times the nucleon-spallation attenuation length ($\frac{\rho}{\Lambda_n}$) and 5% of imposed sample deviation (Table 1). The resulting distributions of the mean age (Fig. 4) are all well centered around the true age even with the largest amount of denudation tested. We also observe that when total denudation reaches 3- and 5-times attenuation length, the ranges of the estimated mean age grow slightly wider, indicating a decrease of precision. This phenomenon can also be observed with the Bayesian approach (Fig. S6), which suggests it is not a result of the approximation introduced through eq. 9. Instead, we suggest this problem relates to low concentration gradient for profiles with a large amount of denudation, making the inversion more sensitive to

measurement error. We find that the distribution of the mean inheritance remains well centered around the true inheritance for all simulated profiles, even for profiles with denudation equal to 5-times attenuation length.

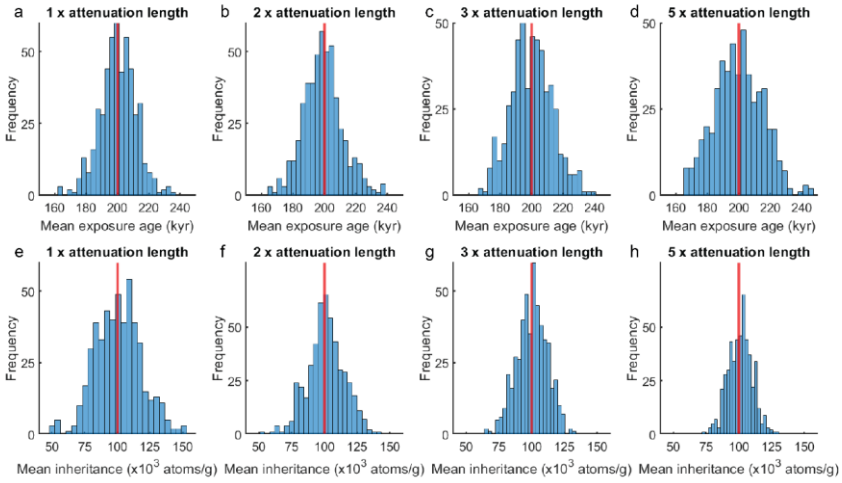

Figure 4 Distribution of mean exposure age (a-d) and inheritance (e-h) estimated from linear regression (eq. 10) for 500 simulated (5000 atoms/g) TCN profiles with 5% of imposed sample deviation and with total denudation equals to 1 (a and e), 2 (b and f), 3 (c and g) and 5-times (d and h) attenuation length of spallation. Red vertical line annotates the true age and true inheritance.

3.1.4 Deep sample profiles

Samples at depths greater than ~2 m are especially sensitive to muogenic production (Fig. 1). Here we test our denudation-depth approximation with depth profile samples distributed between 3 and 5 m depth to mimic the situation when near surface samples are not obtainable. Three groups of profiles, subjected to a total denudation of 0, 2, and 5-times the spallation attenuation length and with 5% of imposed sample deviation, are tested with both linear regression and Bayesian approach (Table 1).

We find that compared to the near-surface profiles, results from the deep profiles show greatly reduced precision, especially for large denudation depths (Fig. 5, S7). The majority (95% confidence) of the mean exposure ages estimated with linear regression spread between 100-300 kyr, 20-400 kyr, and 0-570 kyr, for surfaces with 0, 2, and 5-times attenuation length of denudation, respectively (Fig. 5). This occurs with both linear regression and Bayesian approaches, indicating the precision drop is not due to our approximation of muogenic production (eq. 9). Similar to the examples with large denudation (Fig. 4), we suggest the low precision is a result of the very low concentration gradient at depth. Different from near-surface profiles, a small change in the concentration gradient at depth leads to a large change of the estimated exposure age, which makes the inversion overly sensitive to random scatter of sample concentrations. As a comparison, by setting the imposed sample

deviation to 1% instead of 5%, we find that precision increases greatly (Fig. 6). With linear regression, the majority (95% confidence) of the mean exposure ages are distributed between 180 - 220 kyr, 162 - 242 kyr, and 131-275 kyr for 0, 2, and 5-times attenuation length denudation, respectively (Fig. 6, S8). Thus, theoretically, both linear regression and Bayesian approach can produce accurate estimates if the scatter of sample concentrations is low. Reducing analytical uncertainty through use of large sample masses would be crucial for the success of a deep sample profile.

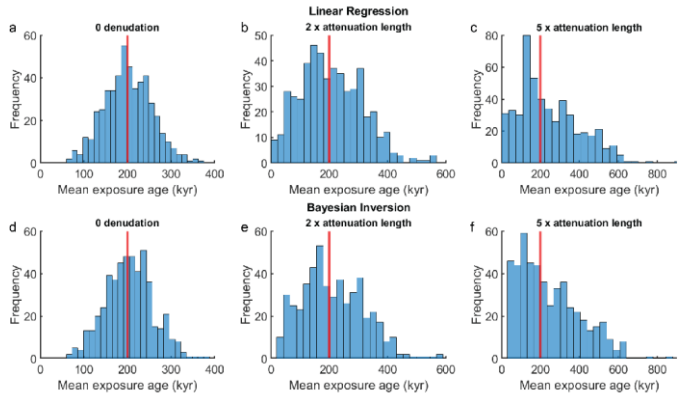

Figure 5 Distribution of age estimations from linear regression (a-c) and a Bayesian approach (d-f) for 500 simulated TCN deep (3-5 m) profiles with denudations equal to 0 (a, d), 2 (b, e), and 5-times (c, f) attenuation length, and with 5% imposed deviation of sample concentration. 500 groups of inversion results.

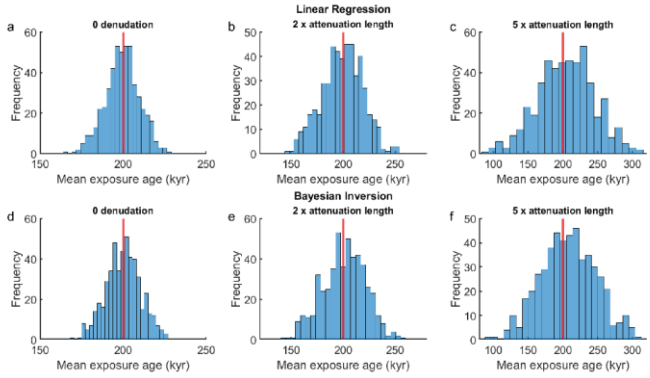

Figure 6 Distribution of age estimations from linear regression (a-c) and a Bayesian approach (d-f) for 500 simulated TCN deep (3-5 m) profiles with denudations equal to 0 (a, d), 2 (b, e), and 5-times (c, f) attenuation length, and with 1% imposed deviation of sample concentration. 500 groups of inversion results.

3.2 Case Examples

Here we present two case examples to show the application of our linear regression model to natural conditions. Wang et al. (2020) excavated a sample pit ~2 m deep beneath the tread of a terrace deposit from the Beida River, within the North Qilian Shan, western China. The site is covered with 125 cm loess which was deposited continuously since 8.3 kyr. Beneath the loess cover, erosional truncation of the A and uppermost B horizon of the soil profile indicates that there may have been 20-60 cm of erosion of the terrace tread prior to the onset of loess accumulation. We collected six samples of medium to coarse sand from up to 2 m below the base of the loess. ~~**Table 2 ^{10}Be concentration prior to (C1) and post (C2) loess accumulation, and the production rate at each sample depth.**~~

~~Sample ID~~	~~Loess cover (cm)~~	~~C_2 (10^4 atoms/g)~~	~~C_1 (10^5 atoms/g)~~	~~P_z ($P_0 e^{-\frac{\rho z}{\Lambda}}$; atom*g^{-1}*yr^{-1})~~
~~BT2-2-20~~	~~130~~	~~7.11 ± 1.58~~	~~14.33 ± 0.39~~	~~13.82 ± 0.91~~
~~BT2-2-45~~		~~5.11 ± 1.14~~	~~9.84 ± 0.36~~	~~9.94 ± 0.65~~
~~BT2-2-75~~		~~3.44 ± 0.77~~	~~5.68 ± 0.23~~	~~6.69 ± 0.44~~
~~BT2-2-110~~		~~2.17 ± 0.48~~	~~4.09 ± 0.21~~	~~4.22 ± 0.28~~
~~BT2-2-150~~		~~1.46 ± 0.33~~	~~2.96 ± 0.11~~	~~2.84 ± 0.19~~
~~BT2-2-180~~		~~0.86 ± 0.19~~	~~2.63 ± 0.08~~	~~1.68 ± 0.11~~

~~**Table 3 Values for parameters used in exposure age calculation.**~~

~~Parameter~~	~~Values (Wang et al., 2020)~~	~~Values (Hidy et al., 2010)~~
~~Surface production rate (nucleon-negative muon-fast muon) (atom*g^{-1}*yr^{-1})~~	~~23.4, 0.259, 0.155~~	~~9.51, 0.145, 0.115~~

Density (g/cm3)	2.2	2.2–2.5 (uniform distribution)
Attenuation (nucleon, negative muon fast muon) (g/cm2)	167, 1500, 5300	160±5, 1500, 5300
Eroded thickness (cm)	40±10 (normal distribution)	0–30 (uniform distribution)
Erosion rate (cm/kyr)	0.3±0.05 (normal distribution)	0–0.32 (uniform distribution)

3.1.2 Exposure age estimation

Because the terrace tread is covered by loess, we need to first estimate the ^{10}Be concentration at the time of the onset of loess accumulation. Follow the approach introduced by Hetzel et al., (2002), the ^{10}Be concentration prior to (C_1) and post (C_2) loess accumulation are calculated and listed in table 2. Parameters we use for inversion are listed in table 3.

Using a normally distributed erosion rate of 0.3±0.05 cm/kyr, we first find the ^{10}Be concentrations for these samples, corrected for loess accumulation using the approach of Hetzel et al. (2004) are listed in table S1.

To explore the effect of denudation rate, we use the most likely concentrations for each sample and invert for a preliminary T_{en} and inheritance values of 99.3 kyr and 8.3×10^3 atoms/g respectively, using eq. 6. Using eq. 7, we generate a plot of exposure age vs. denudation rate based on the preliminary T_{en} value. The plot (Fig. 7) shows that if there has been no denudation, the sample site has a minimum exposure age of ~102 kyr prior to loess accumulation. This exposure age increases to 160 kyr and 240 kyr when the denudation equals to 1 and 2-times the attenuation length, respectively. When the denudation rate reaches ~0.7 cm/kyr, the TCN accumulation and denudation reach equilibrium and no age may be determined.

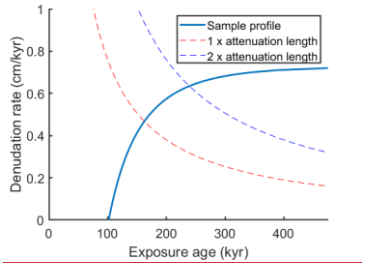

Figure 7 exposure age-denudation rate relationship of the Beida River terrace

To explore the full distribution of potential age and inheritance results, we apply a Monte Carlo sampling of the sample concentrations, depths, denudation depth, etc. (Table S2). Using a normal distribution for the denudation depth with 40 cm as the mean and 10 cm as the standard deviation, we apply least-squares linear inversion with eq. 10. Best-fit results for ^{10}Be concentration (C_1) and effective exposure age (T_{en}) and inheritance (at the time of loess accumulation; C_{inh}) by linear regression

using eq. 6. The best fit line(s) of the data (C_1 and P_{zn}) are shown on figure 2a, the production rate (P_{ze}) are shown on figure 8a, and the corresponding fitted depth profile curves are shown on figure 2b. Because our sample site contains very low inheritance (Figure 2d), some inversion results yield non-physical predictions with negative inheritance. These negative inheritance predictions are necessary to estimate the full distribution of the exposure age, but we exclude these from the final inheritance results. The predicted 95% confidence range of T_{en} and C_{inh} after 100,000 iterations ranges from 86.8 to 111.7 kyr and from -3.4 x 10^4 to +7.12 x 10^4 atoms/g, respectively. Substituting8b. The T_{en} and C_{inh} into eq. 7, the range of the exposure age is 107.6-160.8 kyr (95% confidence) prior to loess accumulation (Figure 2e). The possible range of inheritance is 0-7.12 x 10^4 atoms/g after excluding negative results. The corresponding eroded thickness is 23-59 cm (Figure 2g).

For the eroded-thickness approach, we also assume a normal distribution for the total erosion, and choose 40 cm as the mean and 10 cm as the standard deviation of the eroded thickness. By applying least squares linear inversion with eq. 10, the best fit line(s) of the data (C_1 and P_{ze}) are shown on figure 3a, the fitted depth profile curves are shown on figure 3b. Including the muogenic production pathways into calculation leads to a slightly younger (1% shift of the mean) T_{en} value of 85.9-110.7 kyr and a lower inheritance of -9.1 x 10^4 to +2.9 x inheritance values are 86.4-111.6 kyr and -4.5×10^4 to +6.4×10^4 atoms/g, respectively (ranges correspond to the 95% confidence distributions for each value, figure 3c 3dfigures 8c and 8d). The corresponding exposure age, calculated following eq. 11-13, is 108.3-154.29-155.4 kyr (2σ) prior to loess accumulation (Figure 3e8e). Excluding the negative inheritance results, the possible range of inheritance is 0-2.9 x 6.4×10^4 atoms/g. The corresponding erosion rate is 0.18-0.42 cm/kyr (Figure 3f and 3g).8f and 8g). If we do not permit negative inheritance during the inversion, the resulting exposure age and inheritance would be 107.2-143.9 kyr and 0-4.6×10^4 atoms/g. (2σ) instead. This ~5 kyr shift of the mean age is consistent with the expected effect of excluding negative inheritance during the fitting process.

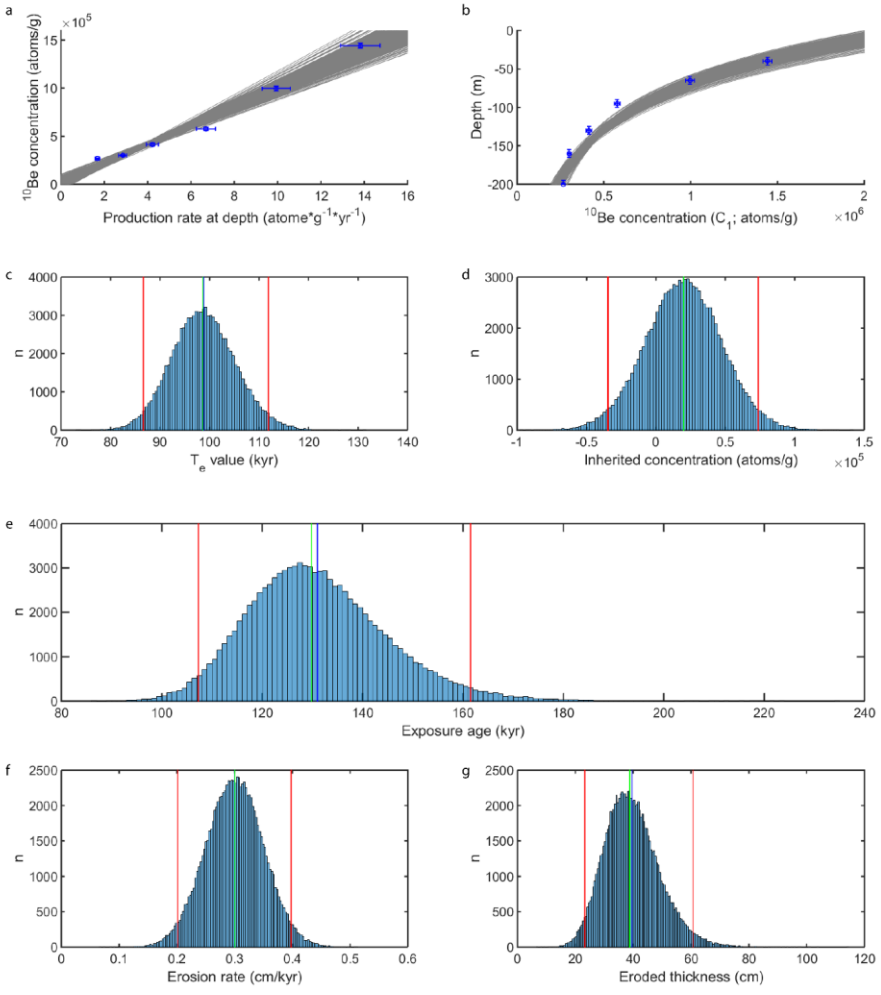
a
^{10}Be concentration (atoms/g)
×10^5
Production rate at depth (atome*g^{-1}*yr^{-1})
b
Depth (m)
^{10}Be concentration (C$_1$; atoms/g)
×10^6
c
n
T$_e$ value (kyr)
d
n
Inherited concentration (atoms/g)
×10^5
e
n
Exposure age (kyr)
f
n
Erosion rate (cm/kyr)
g
n
Eroded thickness (cm)

380

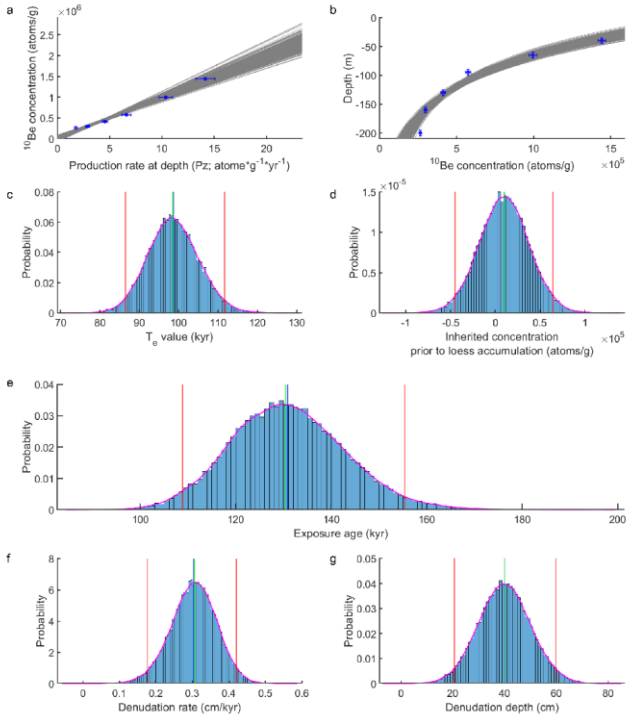

Figure 8 Linear regression results for Beida River T2 terrace ~~data set~~ using ~~the erosion rate~~denudation-depth approach after 100,000 iterations. a. Relationship of sample concentration to production rate at depth. Grey lines are the best fit lines through this data set~~.~~; b. distribution of depth profile models with best fit curves (grey lines). c. Distribution of the effective exposure age (T_e); d. Distribution of the inherited ^{10}Be concentration prior to loess accumulation. e. Distribution of exposure age ~~estimated based on preset erosion rates with T_e value~~estimates derived from T_{en} values from linear regression (Figure ~~2c). f.~~ 8c). f. Distribution of denudation rates predicted by the model; g. Distribution of sampled ~~erosion rates; g. Distribution of~~ total ~~eroded thicknesses predicted by the model.~~denudation-depth. Red lines indicate ~~2σ~~95% confidence ~~error~~ range, green line indicates the median of the distribution, blue line indicates the mean of the distribution.

Hidy et al. (2010) reported a ^{10}Be depth profile from the Lees Ferry site, excavated on top of a Colorado River fill terrace. Based on the soil profile, a total erosion of 0-30 cm is estimated for the sample site. For this site Hidy et al. (2010) applied their Monte-Carlo model and originally reported an exposure age and inheritance of 69.8-103 kyr, and 6.97-10.70 atoms/g, respectively (95% confidence). After updates of their code (v1.2, Hidy et al., 2010; Mercader et al., 2012), including the incorporation of a Bayesian fitting process, their model provides a new age estimation of 76.6-96.1 kyr. See Hidy et al. 2010 for more details of the sample site, sampling and processing, age results interpretation.

Following the original study, we apply our modelling approaches to the sand depth-profile data (Table S1). In order to compare with results reported by Hidy et al.

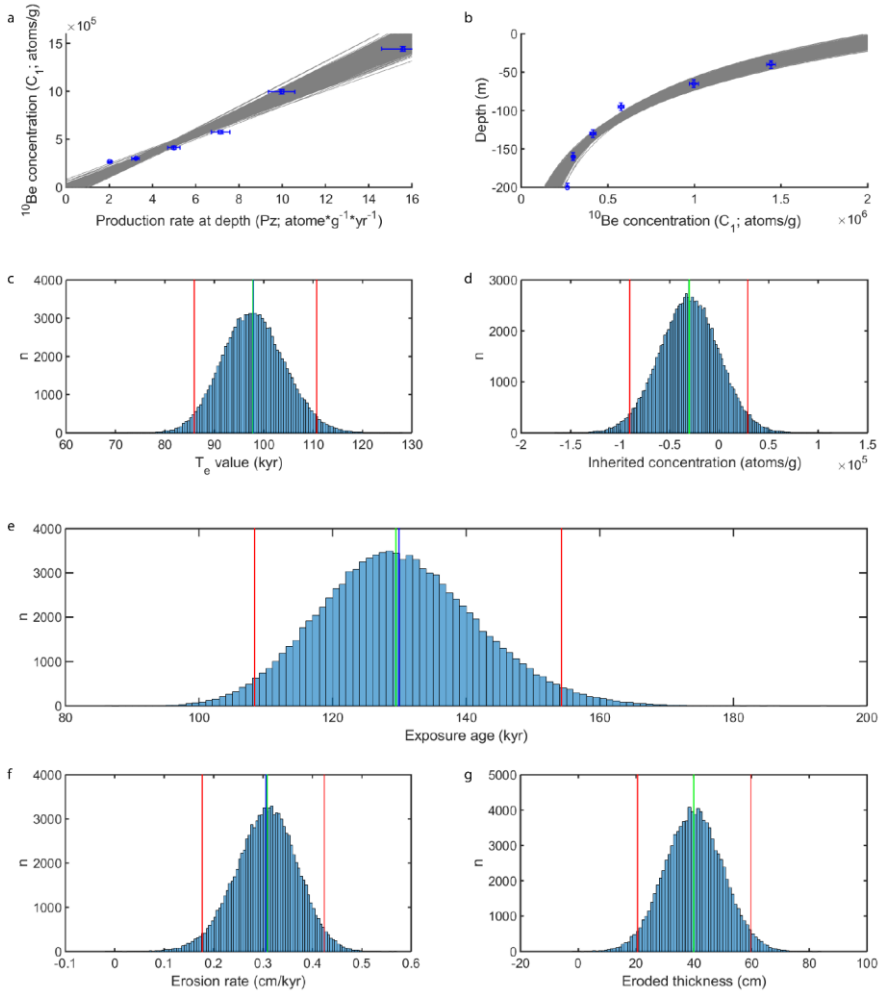

(2010), we use the same values they do for all parameters wherever possible (Table S2). Similar to the Beida River depth profile, we estimate the exposure age with the denudation-depth approach, applying Monte Carlo simulation of the uncertainty

of input parameters. With a uniformly distributed 0-30 cm denudation length, the inverted best fit lines and curves are in figure 9a and 9b. The estimated range of T_e and C_{inh} values are 65.0-79.6 kyr and 7.6-11.4 × 10^4 atoms/g, respectively (95% confidence; Figure 9c and 9d). The estimated exposure age is 70.0-95.5 kyr (95% confidence; Figure 9e).

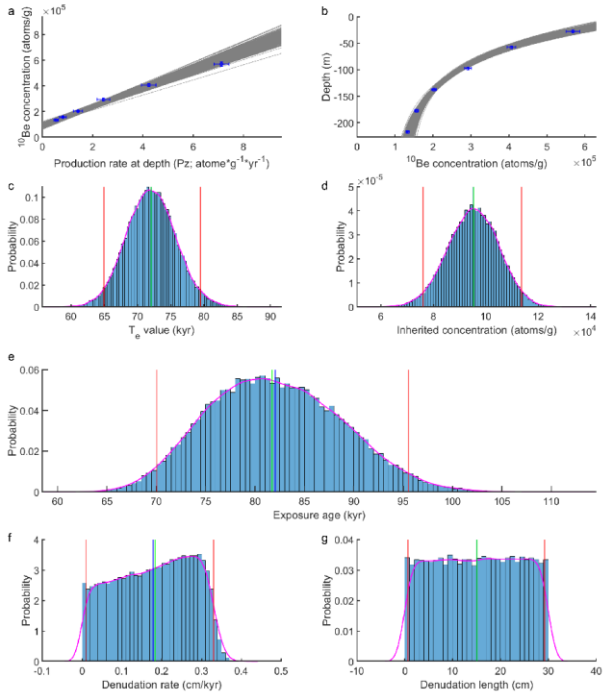

Figure 9 Linear regression results for ~~Beida River T2 terrace using eroded thickness~~Lees Ferry data set with denudation-depth approach after 100,000 iterations. ~~**a. Relationship of sample concentration to production rate at depth. Grey lines are the best fit lines through this data set b. distribution of depth profile models with best fit curves (grey lines). c. Distributions of the effective exposure age (T_e); d. Inherited ^{10}Be concentration prior to loess accumulation. e. Exposure age estimates based on preset erosion rates with known T_e value from linear regression (Figure 3c). f. Distribution of erosion rates predicted by the model; g. Distribution of sampled total eroded thicknesses. Red lines indicate 95% confidence range, green line indicates the median of the distribution, blue line indicates the mean of the distribution.**~~

~~3.2 Lees Ferry Example~~

~~3.2.1 Sample site~~

~~This ^{10}Be depth profile data set was originally reported by Hidy et al. (2010). The sample pit was excavated on top of the M4 (main stem) Colorado River fill terrace at Lees Ferry, Arizona. Based on the soil profile, a total erosion of 0-30 cm is estimated~~

for the sample site. One surface sample and two groups of depth profile samples (a sand profile and a pebble profile) were collected from the pit, but they rejected the results of the pebble profile data, for their poor fit to the depth profile and the estimated age result deviates largely from their independent OSL age constraint. For this site Hidy et al. (2010) applied their model to estimate an exposure age and inheritance of $83.9^{+19.1}_{-14.1}$ kyr, and $9.49^{+1.21}_{-2.52} \times 10^4$ atoms g^{-1}, respectively (95% confidence). The erosion rate of the site was estimated as 0-0.32 cm/kyr. See Hidy et al. (2010) for more details of the sample site, sampling and processing, age results interpretation.

Table 4 Sample information and ^{10}Be concentration of Lees Ferry sample site (Hidy et al., 2010)

Sample ID	Coordinates and elevation	Depth (cm)	Thickness (cm)	Dissolved Quartz (g)	Carrier Mass (g)	Corrected $^{10}Be/^{9}Be$	^{10}Be Concentration (atoms/g)	1s Total Measured Error	P_{ε} (atom*g^{-1}*yr^{-1})
GC-04-LF-404.30s	36.853°N, −111.606°W; 985 m	27.5	5	45.2566	0.308	1.2769E−12	568744	17347	6.35 ± 0.48
GC-04-LF-404.60s		57.5	5	45.9469	0.3	9.5176E−13	406713	11469	4.09 ± 0.48
GC-04-LF-404.100s		97.5	5	50.1042	0.3123	7.1640E−13	292243	8972	2.27 ± 0.39
GC-04-LF-404.140s		137.5	5	51.1421	0.3034	5.2302E−13	203072	6234	1.26 ± 0.29
GC-04-LF-404.180s		177.5	5	55.3693	0.3085	4.3112E−13	157209	4921	0.7 ± 0.2
GC-04-LF-404.220s		217.5	5	55.1112	0.2974	3.7997E−13	134198	3892	0.39 ± 0.13

3.2.2 Exposure age estimation

As in the original study, we apply our modelling approaches to the sand depth-profile data (Table 4). In order to compare with results reported by Hidy et al. (2010), we use the same values as they did for all parameters wherever possible (Table 3). Similar to the Beida River profile, we estimate the exposure age with both erosion-rate and eroded-thickness approaches.

With the erosion-rate approach, we use a uniformly distributed erosion rate of 0-0.32 cm/kyr (Figure 4f). We invert the effective exposure age (T_{en}) and inherited concentration (C_{inh}) based on ^{10}Be production rate and concentration at each sample depth. The best fit lines and curves are in figure 4a and 4b. The estimated range of T_{en} and C_{inh} values are 66.1-79.6 kyr and 9.45-12.82 x 10^4 atoms/g, respectively (95% confidence, Figure 4c, 4d). The estimated exposure age is between 70.5-96.4 kyr (Figure 4e).

With the eroded-thickness approach, we use a uniformly distributed 0-30 cm thickness (Figure 5g). We invert the effective exposure age (T_e) and inherited concentration (C_{inh}) based on effective ^{10}Be production rate (P_{ze}) (eq. 10) and ^{10}Be concentration at each sample depth. The best fit lines and curves are in figure 5a and 5b. The estimated range of T_e and C_{inh} values are 65.7-79.0 kyr and 7.78-11.11 x 10^4 atoms/g, respectively (95% confidence; Figure 5c and 5d). The estimated exposure age is 70.6-95.1 kyr (95% confidence; Figure 5e).

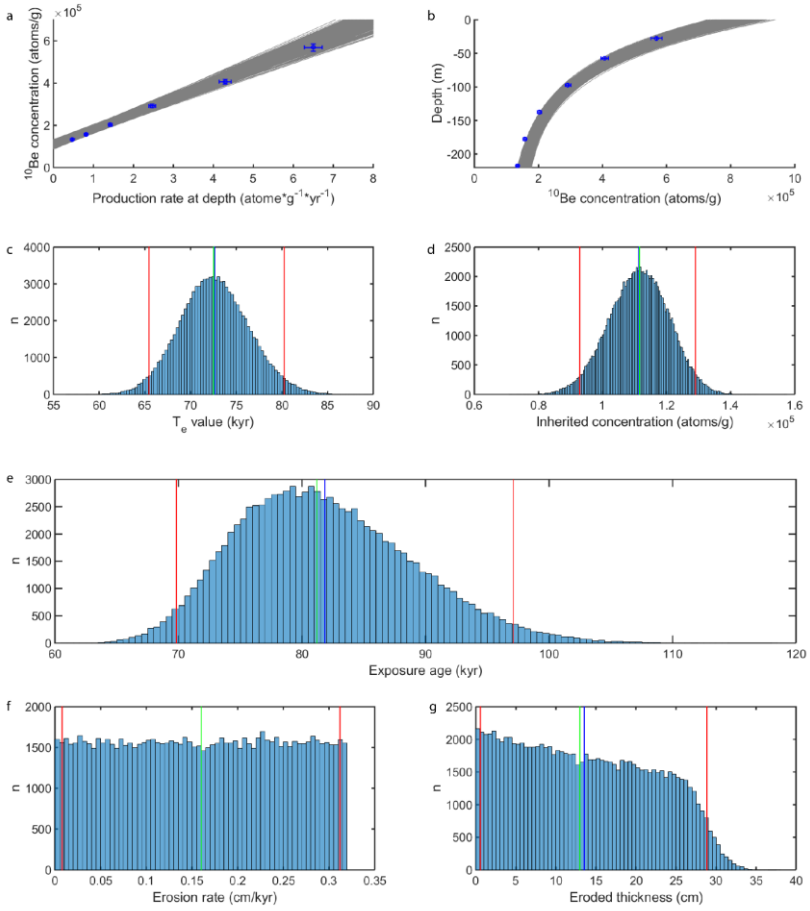

Figure 4 Linear regression results for Lees Ferry data set with erosion-rate approach after 100,000 iterations. a. Relationship of sample concentration to production rate at depth. Grey lines are the best fit lines for the data. b. distribution of depth profile models with best-fit curves (grey lines). c. Distribution of effective exposure age (T_e); d. Distribution of inherited ^{10}Be concentration. e. Exposure age estimated based on preset erosion rates with T_e values derived from linear regression (Figure 4c). f. Distribution of sampled erosion rates. g. Distribution of total eroded thicknesses predicted by the model. Red lines indicate 95% confidence range, green line indicates the median of the distribution, blue line indicates the mean of the distribution.

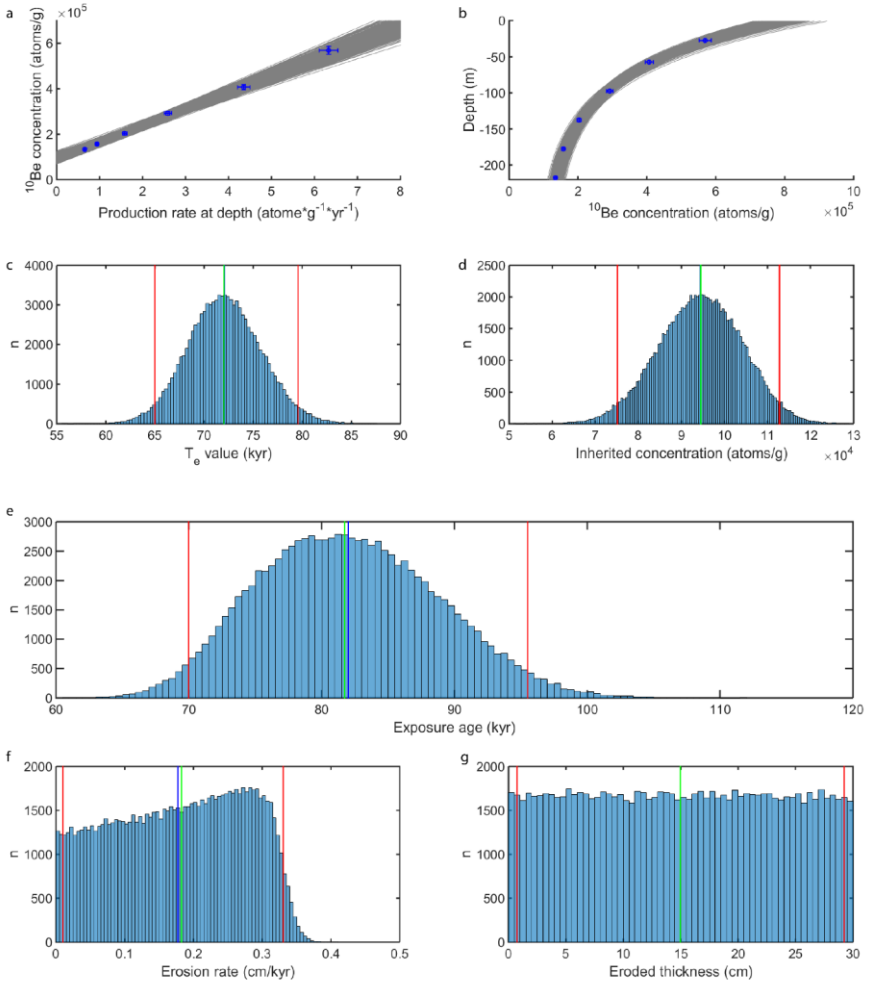

~~Figure 5 Linear regression results for Lees Ferry data set with eroded-thickness approach after 100,000 iterations.~~ a. Relationship of sample concentration to production rate at depth. Grey lines are the best fit lines for the data. b. distribution of depth profile models with best fit curves (grey lines). c. Distribution of the effective exposure age (T_e); d. Distribution of inherited ^{10}Be concentration. e. Distribution of exposure age ~~estimated based on preset erosion rates with T_e values~~ estimates derived from T_e values from linear regression (Figure ~~5c~~9c). f. Distribution of ~~erosion~~denudation rates predicted by the model. g. Distribution preset

of total ~~eroded thicknesses~~denudation-depth. Red lines indicate 95% confidence error range, green line indicates the median of the distribution, blue line indicates the mean of the distribution.

4. Discussion

4.1 ~~Modeled age results~~Case-Example Comparison

For the Beida River ~~T2 terrace, the age prior to loess accumulation estimated with erosion rate is 107.6-160.8 kyr, and~~ site, comparing the age ~~estimated with eroded thickness is~~ determined here (108.~~3-154.2~~9-155.4 kyr~~. Compare~~) to ~~the age~~that we reported previously (107.9-164.5 kyr; Wang et al., 2020), the ~~age estimated here (erosion-rate approach) is slightly~~mean is 3% younger ~~(1.5% shift of the mean age). This shift occurs because the depth distributions for each sample were not sampled independently in the original paper. For the age estimated with the eroded-thickness approach, the mean is 4% younger than in the 2020 paper, .~~ while the 95% error range is ~~19~~18% smaller. These differences come from three different sources. First, there is a ~1.~~5~~% shift that arises from independently sampling depth for each measurement~~.~~ (the depth distributions for each sample were not sampled independently in the original paper). Second, ~~taking~~the original paper did not take muogenic production into account. The contribution from muons leads to slightly younger age ~~estimations~~ and ~~lower~~lowers the inheritance ~~estimations—an issue we explore further below.~~ Third, we applied the denudation-rate approach (eq. 6) in the 2020 paper, and the corresponding ~~erosion~~denudation rate distributions are slightly different for the two approaches ~~(Figure 2f, 3f). Sources 2 and 3 combined leads to 2.5~~. Combined, the addition of muogenic contribution and using a denudation-depth instead of denudation-rate approach leads to ~2% shift of the mean age and to ~~15~~18% narrowing of the error range.

~~It is important to note that, for sites with low inheritance like the Beida River T2 site, permitting negative inheritance results in the resulting distribution is essential to accurately estimating the best-fit exposure age. Truncating the exposure-age distribution by removing negative inheritance results will bias the best-fit age younger because the underlying inheritance distribution will be biased higher. For example, the true age of a surface with zero inheritance would lie to the extreme older tail of such a truncated age distribution, and would thus be excluded at 95% confidence. If instead, negative inheritance results were not discarded, the age true surface age would lie at the expected (mean) value of the full, untruncated distribution. For our realistic example, if we exclude negative inheritance from our age inversion for T2, the resulting exposure age distribution (pre-loess accumulation) would span 101.6-135.1 kyr at 95% confidence, excluding almost 20 kyr from the older tail. The best-fit age value declines by ~10% in the truncated distribution. We further note that this issue related to low inheritance samples not only affects our least squares inversions, but also affects other exposure-age estimation approaches.~~

~~For the Lee's Ferry site, our age estimations of 71.0-96.4 kyr (erosion-rate approach) and 70.5-95.0 kyr (eroded-thickness approach) are very similar to each other, with the erosion-rate age slightly older due to the exclusion of muogenic production. These estimates generally agree with Hidy et al. (2010)'s result, 69.8-103 kyr, but the uncertainty at 95% confidence is smaller with our inversion-based Monte-Carlo approach. We suggest this arises from differences between the two approaches. Specifically, though both methods attempt to minimize sum of the squares of the residuals, the least squares linear inversion~~

~~samples C, r, and z, and the inversion only finds one set of best-fit t and Cinh from each sample. Conversely, the forward-model χ^2 minimiziation approach employed by Hidy et al. (2010) randomly samples t, and Cinh, in addition to r and z values from proposed ranges then calculates the χ^2 values to find the sets of results that fall within 95% confidence of measured concentration data. The inheritance estimated using our erosion-rate approach is 9.45-12.82 x 10^4 atoms/g, which is significantly larger than Hidy et al. (2010)'s result, 6.97-10.7 x 10^4 atoms/g. This is mainly because the erosion-rate inversion (~~For the Lees Ferry site, our age estimation of 70.0-95.5 kyr using denudation depth approach generally agrees with the result reported by Hidy et al. (2010), 69.8-103 kyr (or 76.6-96.1 kyr based on recalculation with updated v1.2 code), though small discrepancies in mean age and 95% confidence range remain between the two approaches. We suggest this arises from two different sources. First, as demonstrated in section 3.1.1 and figures S1-3, most of the discrepancy may be due to differences between the least-squares and Bayesian model. Secondly, we use a two-term approximation for muogenic process in our model instead of a 5-term approximation used in the original study (Hidy et al., 2010), which may lead to a minor estimation discrepancy.

4.2 Sources of error

~~eq. 6) does not account for muogenic ^{10}Be. On the other hand, the inheritance estimated using our eroded-thickness approach is 7.78-11.11 x 10^4 atoms/g, which is only slightly larger than Hidy's result. We attribute this difference to the slightly narrower range of best-fitting exposure age estimates found using our inversion approach.~~

4.2 ~~Sources of Error~~.1 Denudation

~~4.2.1 Surface erosion~~

~~Surface erosion~~Denudation and its uncertainty constitute a major source of error in exposure age estimation. With the same surface ^{10}Be concentration, higher ~~erosion~~denudation rate and/or larger ~~eroded thickness~~denudation depth would result in an older effective surface age (e.g. Figure 1). If a surface is sufficiently old, or if the ~~erosion~~denudation rate is sufficiently high, the ~~CN~~TCN build up at surface will reach equilibrium with nuclides removed through erosion (Lal, 1991). Figure ~~6a~~10a shows the relationship between ~~erosion rates~~denudation rate and surface ~~ages.~~age (Eq. 7). This figure suggests that once the ~~eroded thickness~~denudation depth exceeds the mean attenuation length of nucleon spallation ($\frac{\Lambda_n}{\rho}$), the slope of the age versus erosion rate relationship ~~decreases so as to make~~degrades the age determination ~~poor~~. Once the ~~eroded thickness~~denudation depth exceeds twice of the attenuation length of spallation, the age versus ~~erosion~~denudation rate curve flattens so much that it becomes effectively impossible to estimate surface age~~.~~ using a denudation-rate approach. On the other hand, the age-~~eroded thickness~~denudation depth curve does not flatten as much (Figure ~~6b~~10b), and therefore it is theoretically possible to use the ~~eroded thickness~~denudation depth to determine surface age even when total ~~erosion~~denudation exceeds twice of the attenuation length. Our simulated depth-profile analysis also shows that the denudation-depth approach can provide accurate estimations even with denudation reaches 5 times spallation attenuation length. In practice, however, surfaces with such a large amount of

~~erosion~~denudation would subject to large uncertainties and the ~~erosion~~denudation history may be too complex for the constant ~~erosion~~denudation rate assumption, which underlies both approaches, to be valid, casting doubt on the utility of ^{10}Be exposure dating for such cases.

~~Erosion~~Denudation affects the uncertainty of exposure age estimation in two different ways. First, the uncertainty on the final age ~~gets larger as the erosion rate or thickness~~ increases with denudation rate or depth because of the non-linear relationship between age and ~~erosion rate or thickness~~denudation (Figure ~~6~~10). Second, the age uncertainty will increase further through propagation of the uncertainty of the ~~erosion rate~~denudation. This suggests that when excavating depth profile pits in surfaces subject to ~~erosion~~denudation, it is crucial to document surface texture and analyze the soil profiles to estimate ~~eroded thickness~~denudation depth, for a small deviation from the true ~~erosion~~denudation rate or depth would lead to a large bias in the resulting exposure age. (Ebert et al., 2012; Frankel et al., 2007; Hidy et al, 2010; Mercader et al., 2012; Ruszkiczay-Rüdiger et al., 2016).

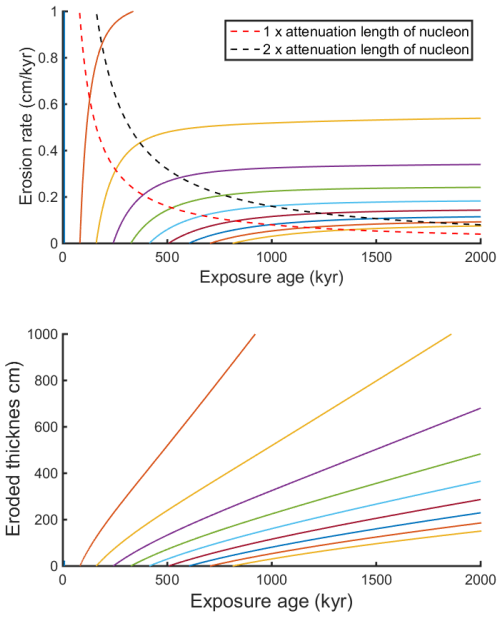
1 x attenuation length of nucleon
2 x attenuation length of nucleon
Erosion rate (cm/kyr)
Exposure age (kyr)
0
0.2
0.4
0.6
0.8
1
0
500
1000
1500
2000

Eroded thicknes cm)
Exposure age (kyr)
0
200
400
600
800
1000
0
500
1000
1500
2000

525

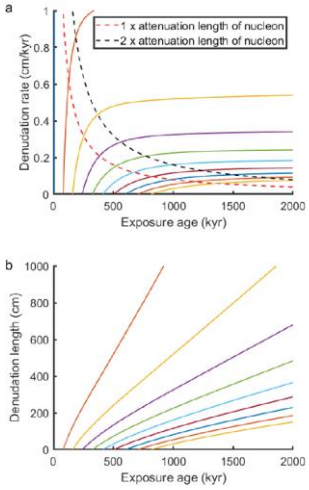

Figure 10 a. The relationship between ~~erosion~~denudation rate and exposure age. Each colored line representing the age-~~erosion~~denudation relationship of a specific depth profile (or surface concentration). b. The relationship between ~~eroded thickness~~denudation depth and exposure age; the color coding ~~is similar to fig. 6a. The parameters used for this simulation are: matches~~ scenarios shown in ~~a total production rate of 15 atoms/g, a density of 2 g/cm^3; the relative contributions of nucleons and muons (negative and fast) to the total ^{10}Be production were 97.85%, 1.5% and 0.65%, the relative attenuation lengths are 160 g/cm^3, 1500 g/cm^3 and 5300 g/cm^3.~~.

4.2.2 ~~Radioactive decay~~

~~For CNs such as ^{10}Be, the actual exposure age, t, is always larger than the effective exposure age, T_e, due to radioactive decay (eq. 5). The error resulting from ignoring decay grows larger as the surface age increases (Figure 7). For young surfaces (<200 ka) with zero erosion, excluding radioactive decay underestimates the age by less than 5 %. For older surfaces, i.e., a surface with an age of 1 Myr, ignoring radioactive decay would result in ~30 % of underestimation. All of the approaches developed in this paper take decay into account.~~

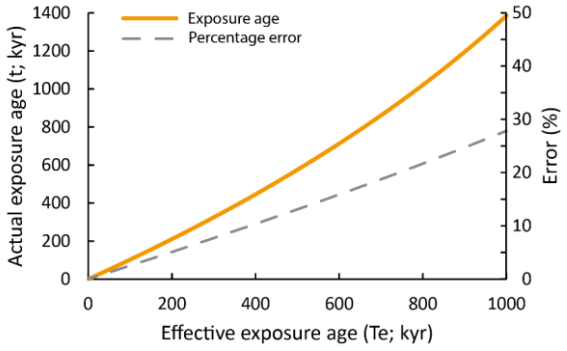

~~Figure 7 The relationship between actual and estimated exposure age when radioactive decay is ignored.~~

~~4.2.3~~ Muogenic production

Muogenic production affects the accuracy of the estimated surface ages differently for the various approaches considered here. For surfaces with no ~~erosion~~denudation, muons may be fully incorporated into the inversion (eq. 4), therefore the uncertainty only comes from the uncertainties of parameters related to muogenic production (attenuation length and production rate). ~~Ignoring~~When denudation is present, both denudation-rate and denudation-depth approaches come with error related to muons. For the denudation-rate approach, which ignores muons and only ~~relying~~models on the relationship between ^{10}Be concentration and ~~the~~ nucleon spallation production rates (~~Anderson et al., 1996) leads to~~eq. 6), there is a slight overestimation of exposure age and inheritance. ~~A demonstration of this effect is shown on figure 8a. By ignoring muons (treating the total concentration as the result of nucleon spallation and inheritance), the line fitting the P_{sn} vs. C data shifts upward and becomes slightly (and hardly recognizably) steeper (Figure 8a).~~ This is because the inversion process attributes a small portion of the muogenic concentration to nucleon spallation, and a larger portion is attributed to inheritance. ~~When surface erosion is present, muogenic production plays a larger role determining the age (Figure 1b). In fact, with the erosion-rate approach, the error due to ignoring muons grows exponentially with erosion rate (Figure 8b~~For the denudation-depth approach, there is a negligible error related to the approximate solution for the muogenic contribution (Appendix A).

To ~~further investigate how erosion affects age and inheritance estimates, with or without inclusion of muogenic production, we compute exposure ages under five different erosional conditions: total eroded thickness equivalent to 0.5, 1, 2, 3, and 5 times the mean attenuation length for spallation (Figure 9). It is worth noting that 3 and 5 times the mean attenuation length for spallation are included as a theoretical analysis; we do not recommend exposure dating for surfaces with such large eroded thicknesses. With the erosion-rate approach, which omits muogenic production,~~evaluate the error related to muogenic production, we generate profiles with various exposure ages and denudation amounts and compare the estimated results with the true values (Fig. 11). We set the contribution of muogenic production to total surface production as 2%, though in reality

the contribution of muons in most places on earth is smaller (Braucher 2011, 2013; Balco 2008, 2017); therefore, the errors presented here can be treated as a maximum. We find the error introduced by ignoring muons with the denudation-rate approach is relatively small (less than 2% and 5% of overestimate) when the total ~~erosion~~denudation is under one~~-~~ or two-times attenuation length for spallation~~. The age error increases to just under 5% when the total erosion increases to two times the~~ (Figure 11a). Above three-times this attenuation length~~ (Figure 9a). Above this amount of erosion~~, the error grows drastically until no meaningful result can be found~~ with this approach. The eroded-thickness approach, which includes an approximate solution for the muogenic contribution (Appendix A), reduces the error considerably (Figure 9b).~~. Compared to the ~~erosion~~denudation-rate approach, the ~~eroded-thickness approach provides very accurate age estimations even with a large amount of erosion.~~

~~To assess errors for inheritance, we factor out production rate and express inheritance error in terms of years.~~denudation-depth approach reduces the error by at least one order of magnitude (Figure 11b); even with very large total denudation (five times the attenuation length), the error is smaller than 0.3%. Like exposure age, the error in estimated inheritance is related to ~~surface erosion~~denudation and exposure age~~, but the error range is not proportional to mean inheritance~~. As demonstrated in figure ~~9c and 9b,~~11c the ~~amount~~overestimation of ~~error~~ inheritance from the denudation-rate approach increases with the surface age, but slightly decreases as the denudation increases. As a comparison, the amount of error from the denudation-depth approach (Fig. 11d) is one order of magnitude smaller ~~for the eroded-thickness approach compared to the erosion-rate approach. It is worth noting that the errors discussed herein are calculated based on an idealized depth profile, such that all the sample concentrations perfectly fit the expectation. In practice, natural variation of measurements about the expectation leads to larger errors than this idealized case.~~

~~Reassessing our age estimates for the Beida River T2 terrace, the ~2.5% difference between the means of the exposure age estimated with muon-included (eroded thickness) and muon-omitted (erosion rate) approach is slightly larger~~ than ~~our idealized model predicts (~1%). For the Lees Ferry site, we find less than 1% difference between the ages estimated with or without muon contributions, matching the expectations from our hypothetical example (~0.5%).~~the denudation-rate approach.

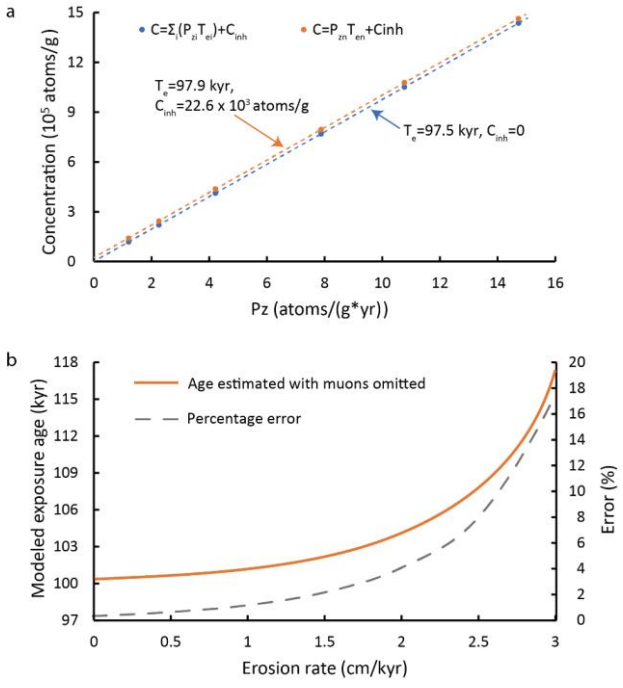
a
C=Σi(Pzi·Tei)+Cinh
C=Pzn·Ten+Cinh
Te=97.9 kyr,
Cinh=22.6 x 10³ atoms/g
Te=97.5 kyr, Cinh=0
Concentration (10⁵ atoms/g)
Pz (atoms/(g*yr))
b
Age estimated with muons omitted
Percentage error
Modeled exposure age (kyr)
Error (%)
Erosion rate (cm/kyr)

585

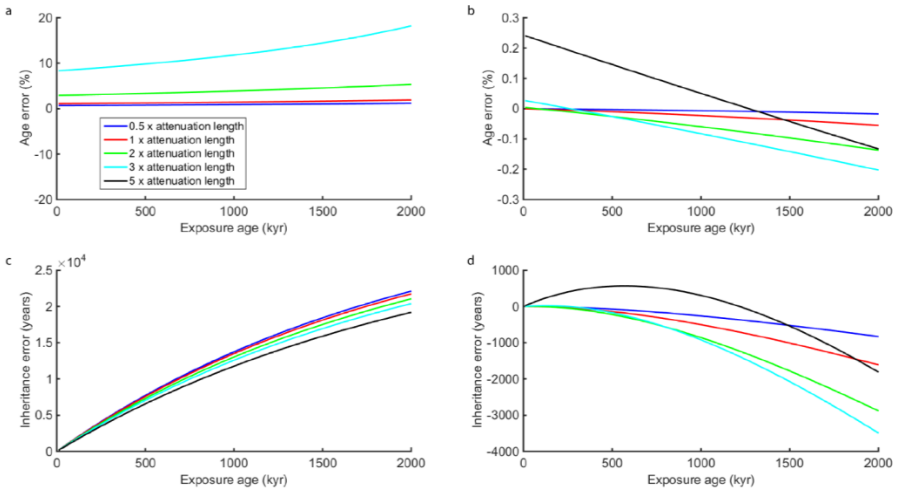

Figure 11 ~~Case study illustrating the solutions for a surface exposed for 100 kyr; a. best fit lines for the surface with zero erosion rate, data same as table S1. b. Modeled exposure ages (left) and model error (right) versus erosion rate. The parameters used for this simulation are: a total production rate of 15 atoms/g, a density of 2 g/cm^3; the relative contributions of nucleons and muons (negative and fast) to the total ^{10}Be production were 97.85%, 1.5% and 0.65%, the relative attenuation lengths were 160 g/cm^2, 1500 g/cm^2 and 5300 g/cm^2.~~

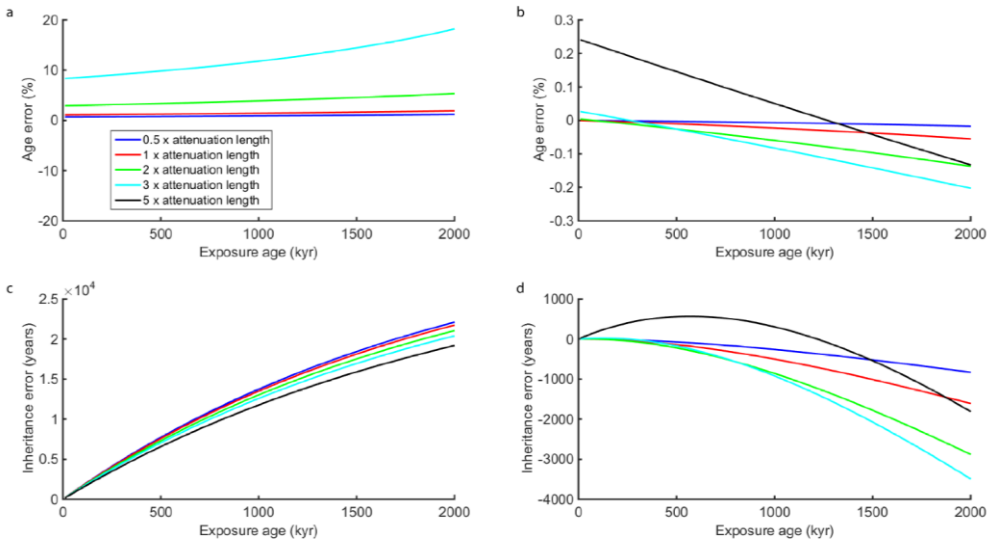

~~Figure 9 Degrees of errors.~~ Error **vs.** ~~exposure age show the advantage of the eroded-thickness approach with approximate solution for muogenic production (b and d) over the erosion-rate approach without muogenic production (a and c).~~exposure age under five different denudation conditions. **Each line represents a modeled surface that has undergone various exposure times, but with the same total** ~~eroded thickness~~denudation**, expressed as a multiple of the attenuation length,** $\frac{\rho}{\Lambda_n}$**. for spallation (see legend). a.** ~~Age~~percentage **error** ~~using erosion~~in exposure age resulting from application of denudation**-rate approach** ~~(eqs. 6-7),~~. Note that **when total erosion reaches 5 times attenuation length, no meaningful result can be found**~~;~~ using this technique. **b.** ~~Age~~percentage **error** ~~using eroded thickness~~in exposure age resulting from application of denudation-depth **approach** ~~(eqs. 8-13);~~. **c.** ~~Inheritance~~ **error** ~~(~~in inheritance, **expressed in** ~~concentration divided by~~ years based on surface production rate, resulting from application of denudation-rate approach. **d. error in inheritance, expressed in years based on surface production rate**~~) using erosion-rate approach; d. Inheritance error using eroded-thickness approach. The relative contributions of nucleons and muons (negative and fast) to the total ^{10}Be production are 97.85%, 1.5% and 0.65%, with Λ equal to 160 g/cm^2, 1500 g/cm^2 and 5300 g/cm^2, respectively (Braucher et al., 2003).~~, resulting from application of denudation-depth approach.

4.2.~~4 Trade-offs between error sources and age estimation~~

~~In previous sections, we discussed how erosion rates, radioactive decay, and muogenic production each individually affect exposure age estimates and error. In general, the muogenic ^{10}Be production contributes least to the uncertainties related to surface exposure dating, compared to the effects of neglecting decay and, especially, the impact of erosion. We show here that radioactive decay may be easily corrected for after finding the effective age with linear regression (3eq. 5, 7, 11-13). Surface erosion, and its uncertainty, thus generally constitutes the largest source of uncertainty for surface-exposure dating.~~

~~With the erosion-rate approach, the degree of error depends on the surface age, and more importantly, the total amount of surface erosion. This method is simple and accurate enough for most exposure age applications (Figure 6a, 9a). When total~~

~~erosion exceeds one to two attenuation lengths, however, the erosion-rate approach is either unable to produce meaningful results, or the uncertainty would be too large (Figure 6a). The eroded-thickness approach is slightly more complex, but also more accurate than the erosion-rate approach, because it incorporates the muogenic contribution. Our approximation of the muogenic contribution (eq. 9; figure 9b) is very robust even with a large total erosion depth. Consequentially, the inheritance estimation is also more accurate with the eroded-thickness approach (Figure 9c, 9d).~~

~~As we show on fig. 6, a small change of erosion rate or eroded thickness may lead to large differences in surface age estimation, especially for the erosion-rate approach. Therefore, we suggest when dating surfaces with erosion, careful examination of the soil profile or other independent evidence of surface preservation is necessary to provide the best constraint possible on the erosion depth. In addition, it is important to consider the assumption of a constant erosion rate at the sample site. It is entirely possible that a sample site may have experienced episodic erosional episodes instead of constant erosion rate, which would lead errors in the age not accounted for in the methods described here.~~

~~4.2.5~~ Other sources of error

As demonstrated with the Beida River sample site and the simulated profiles, low inheritance may lead to underestimation of the exposure age if negative inheritance is not permitted during inversion. Negative inheritance, though physically unreasonable, may be predicted because of the uncertainties within the sample measurements and other parameters related to the TCN concentration. When a profile exhibits very low inheritance, the estimated distribution of the exposure age should center around the true age, with approximately half of the estimated older ages correlated to lower, and possibly negative inheritance, and the other half younger ages correlated to higher, positive inheritance. Imposing a boundary that prevents negative inheritance will lead to a shift of the inheritance distribution to a positive value, which will in turn lead to a shift of the estimated age distribution to younger values. Therefore, when dealing with surfaces with very low inheritance, extra caution is needed when setting boundaries for the inheritance. We suggest permitting negative inheritance when performing a linear regression to avoid underestimation of the age and overestimation of the inheritance. A second-best choice is not to permit negative inheritance when perform a linear regression (i.e. setting inheritance to zero for these cases), while excluding the results with negative inheritance would lead to the most severe underestimation of the exposure age.

Additional sources of error exist for TCN depth-profile ages that we do not consider in this study. Time-dependent phenomena are not considered ~~in our models may further bias age results~~. Constant production rate is an important assumption needed to simplify the nuclear build up process to apply a linear regression approach. In fact, the production rate is time dependent because the strength of Earth's magnetic field varies with time (Balco, 2017; Desilets et al., 2006; Dunai, 2001; Lifton et al., 2005; Stone, 2000). Extending our model to account for temporally variable production rate is beyond the scope of present study. Constant inheritance ~~is another~~and a single value for sediment density are other key ~~assumption.~~assumptions for our approach. Sediments sampled from depth profiles are assumed to be well mixed at the time of deposition and to have been deposited rapidly, such that the inherited concentration and density should be the same at every depth. This ~~may~~will not be

true for sites with incremental deposition, and for sites where the depositional process or catchment-wide ~~erosion~~denudation rates vary with time.

5 Conclusions

~~In this paper,~~ We introduce a ~~combined~~ least-squares linear inversion ~~and Monte-Carlo~~ approach to solve cosmogenic nuclide concentration depth profiles for surface exposure age and inheritance, considering ~~erosion~~denudation rate, ~~erosion~~denudation depth, and muogenic production~~, and radioactive decay. Compared to existing models, our inversion approach offers a simple and direct way to estimate exposure ages, avoiding the non-linear effects of including the full muogenic production pathways where not warranted. In addition,~~. This method allows propagation of ~~all~~ error sources using Monte-Carlo sampling to infer full probability distributions of age and inheritance. In addition, our model presents a straightforward way to assess the trade-offs between exposure age and denudation rate.

~~Comparison of exposure ages estimated using our inverse models with the forward model of Hidy et al. (2010) confirms the robustness of our techniques, especially if using the eroded-thickness approach that includes muogenic production. The example of the Beida River T2 terraces shows that for sites with low inheritance, it is important include negative inheritance into the inversion process in order to fully characterize the distribution of the exposure age. Uncertainty analysis shows that the methods presented here yield suitable ages for surfaces with a total erosion thickness under two times attenuation length. It is likely, however, that this level of erosion may not be well constrained and this ultimately sets a practical upper limit on the applicability of the CN technique for age-dating of depositional landforms.~~

Based on the inversion results of simulated profiles, we show that the least-squares linear regression is a robust approach suitable for most exposure dating scenarios. The accuracy of linear inversion is comparable to a Bayesian approach for most circumstances, except for the more deviated (nosier) sample sets. Importantly, neither inversion approaches consistently outperforms the other.

For surfaces with no denudation, the inversion is using eq. 4 provides an exact solution. For surfaces with denudation, the approximation of mueogenic production using denudation-depth approach (eq. 10) introduces negligible error even for surfaces with a large amount of denudation. The denudation rate approach (eq. 7), though less accurate, provides a useful tool to explore exposure rate vs. denudation rate relationship. Examples of deep profiles suggest that the linear inversion approach works equally well for samples that collected deeper than 2 m from the surface, with or without denudation. However, extra caution is needed when collecting and analyzing deep samples to minimize measurement error, as the resulting ages are much more sensitive to the scatter of concentration values relative to near-surface profiles.

Regardless of whether employing linear regression or a Bayesian approach, surfaces that have undergone a large amount of denudation will be subjected to large uncertainties related to the denudation rate or depth. It also becomes more tenuous in

such cases to assume that the denudation rate was constant throughout the history of the deposit. It is entirely possible that a sample site may have experienced episodic erosional episodes instead of constant denudation rate, which would lead to errors in the age not accounted for in the methods described here.

Appendix A

When ~~r~~ε>0, the effective exposure age T_e takes the following form,

$$T_{ei} = \left(\frac{1-e^{-\left(\frac{\rho r}{\Lambda_r}+\lambda\right)t}}{\frac{\rho r}{\Lambda_r}+\lambda}\right)\left(\frac{1-e^{-\left(\frac{\rho\varepsilon}{\Lambda_i}+\lambda\right)t}}{\frac{\rho\varepsilon}{\Lambda_i}+\lambda}\right) = \frac{1-e^{-B_i t}}{B_i}, B_i = \frac{\rho r}{\Lambda_r}\frac{\rho\varepsilon}{\Lambda_i} + \lambda, i = n, m1, m2. \quad \text{(A1)}$$

This suggests values for T_e value are functions of both ~~r~~ε and t for different production pathways. Between the two variables, ~~r~~ε may be known, while t is unknown. Therefore, our aim is to rewrite A1 into an approximate form where t can be isolated.

We first take a natural logarithm of the T_{em} over T_{en} ratio

$$ln\left(\frac{T_{em}}{T_{en}}\right) = ln\left(\frac{\frac{1-e^{-B_m t}}{B_m}}{\frac{1-e^{-B_n t}}{B_n}}\right) = ln\left(\frac{\frac{1-e^{-B_m t}}{B_m t}}{\frac{1-e^{-B_n t}}{B_n t}}\right) = ln\left(\frac{1-e^{-B_m t}}{B_m t}\right) - ln\left(\frac{1-e^{-B_n t}}{B_n t}\right) \quad \text{(A2)}$$

The expansion of a function, $f(x) = ln\left(\frac{1-e^{-x}}{x}\right)$, $x = B_i t$, in A2 may be achieved by writing a Maclaurin series with the following form

$$f(x) = f(0) + f'(0)x + \frac{f''(0)}{2!}x^2 + \cdots \frac{f^{(k)}(0)}{k!}x^k + \cdots \quad \text{(A3)}$$

To write the expansion, we first rewrite f(x) as

$$f(x) = ln\left(\frac{1-e^{-x}}{x}\right) = ln\left(\frac{1-\left(1-x+\frac{x^2}{2!}-\frac{x^3}{3!}+\frac{x^4}{4!}-\cdots\right)}{x}\right) = ln\left(1-\frac{x}{2!}+\frac{x^2}{3!}-\frac{x^3}{4!}+\cdots\right) \quad \text{(A4)}$$

In this form, f(x) goes to zero when x goes to zero, therefore we have

$$f(0) = ln(1) = 0 \quad \text{(A5a)}$$

$$f'(x) = \frac{-\frac{1}{2}+\frac{x}{3}-\frac{x^2}{8}+\cdots}{1-\frac{x}{2!}+\frac{x^2}{3!}-\frac{x^3}{4!}+\cdots} \text{ and } f'(0) = \frac{-\frac{1}{2}}{1} = -\frac{1}{2} \quad \text{(A5b)}$$

$$f''(x)\left(1-\frac{x}{2!}+\frac{x^2}{3!}-\frac{x^3}{4!}+\cdots\right) + f'(x)\left(-\frac{1}{2}+\frac{x}{3}-\frac{x^2}{8}+\cdots\right) = \frac{1}{3}-\frac{x}{4}+\cdots \text{ and } f''(0) = \frac{1}{12} \quad \text{(A5c)}$$

We omit higher order derivatives from the series expansion.

⋮

Bring A5 into A3, we have the expansion of f(x) as

$$f(x) = -\frac{x}{2}+\frac{x^2}{24}+O(x^3) \quad \text{(A6)}$$

Bringing A6 into A2, the natural logarithm of T_{em} over T_{en} ratio is

$$ln\left(\frac{T_{em}}{T_{en}}\right) = ln\left(\frac{\frac{1-e^{-B_m t}}{B_m}}{\frac{1-e^{-B_n t}}{B_n}}\right) = ln\left(\frac{1-e^{-B_m t}}{B_m t}\right) - ln\left(\frac{1-e^{-B_n t}}{B_n t}\right) = -\frac{B_m t}{2} + \frac{(B_m t)^2}{24} - \left(-\frac{B_n t}{2} + \frac{(B_n t)^2}{24}\right) + \left(O((B_m t)^3) - O((B_n t)^3)\right)$$

(A7)

The contribution of the third, t^3 term, is negligible and may be neglected. Making the substitution D = ~~ri~~et, the first-order terms in A7,

$$-\frac{B_m t}{2} + \frac{B_n t}{2} = -\frac{1}{2}\left(\frac{\rho D}{\Lambda_m} + \lambda t - \frac{\rho D}{\Lambda_n} - \lambda t\right) = -\frac{1}{2}\left(\frac{\rho D}{\Lambda_m} - \frac{\rho D}{\Lambda_n}\right). \quad \text{(A8)}$$

This result is independent of the exposure age, t.

With the same substitution, the second-order terms in A7,

$$\frac{(B_m t)^2}{24} - \frac{(B_n t)^2}{24} = \frac{1}{24}\left[\left(\frac{\rho D}{\Lambda_m} + \lambda t\right)^2 - \left(\frac{\rho D}{\Lambda_n} + \lambda t\right)^2\right] = \frac{1}{24}\left[\left(\frac{\rho D}{\Lambda_m}\right)^2 + \frac{2\rho D\lambda t}{\Lambda_m} + (\lambda t)^2 - \left(\frac{\rho D}{\Lambda_n}\right)^2 - \frac{2\rho D\lambda t}{\Lambda_n} - (\lambda t)^2\right] = \frac{1}{24}\left[\left(\frac{\rho D}{\Lambda_m}\right)^2 - \left(\frac{\rho D}{\Lambda_n}\right)^2\right] + \frac{1}{24}\left[\frac{2\rho D\lambda t}{\Lambda_m} - \frac{2\rho D\lambda t}{\Lambda_n}\right]. \quad \text{(A9)}$$

In equation A9, the first term of the right-hand side is independent of age, t, while the second term is dependent of age. We therefore choose to omit the second term of equation A9 in order to develop an age-independent approximation. We find that this term may be omitted for two reasons. First, the absolute value of A8 is at least one order of magnitude larger than A9, therefore omitting one term from A9 will not lead to significant decrease of accuracy of the overall approximation. Second, for young surfaces, λt is sufficiently small that the second term of A9 is much smaller than the first term, which means omitting it will lead to even smaller decrease of accuracy.

Therefore, an approximate form of the eq. A7 that is independent of t is

$$ln\left(\frac{T_{em}}{T_{en}}\right) \approx -\frac{1}{2}\left(\frac{\rho D}{\Lambda_m} - \frac{\rho D}{\Lambda_n}\right) + \frac{1}{24}\left[\left(\frac{\rho D}{\Lambda_m}\right)^2 - \left(\frac{\rho D}{\Lambda_n}\right)^2\right] \quad \text{(A10)}$$

and the ratio between muon and nucleon effective age can be approximated as

$$\frac{T_{em}}{T_{en}} \approx e^{-\frac{1}{2}\left(\frac{\rho D}{\Lambda_m} - \frac{\rho D}{\Lambda_n}\right) + \frac{1}{24}\left[\left(\frac{\rho D}{\Lambda_m}\right)^2 - \left(\frac{\rho D}{\Lambda_n}\right)^2\right]} \quad \text{(A11)}$$

Acknowledgments and data availability

This work was supported by the US National Science Foundation [grant number EAR-1524734] to Michael Oskin, and through Cordell Durrell Geology Field Fund to Yiran Wang. We placed our code at GitHub (https://github.com/YiranWangYR/10BeLeastSquares).

References

Anderson, R. S., Repka, J. L. and Dick, G. S.: Explicit treatment of inheritance in dating depositional surfaces using in situ 10Be and 26Al, Geology, 24(1), 47–51, 1996.

Balco, G.: Production rate calculations for cosmic-ray-muon-produced 10Be and 26Al benchmarked against geological calibration data, Quat. Geochronol., 39, 150–173, doi:10.1016/j.quageo.2017.02.001, 2017.

Balco, G., Stone, J. O., Lifton, N. A. and Dunai, T. J.: A complete and easily accessible means of calculating surface exposure ages or erosion rates from 10Be and 26Al measurements, Quat. Geochronol., 3(3), 174–195, doi:10.1016/j.quageo.2007.12.001, 2008.

Braucher, R., Brown, E. T., Bourlès, D. L. and Colin, F.: In situ produced 10Be measurements at great depths: Implications for production rates by fast muons, Earth Planet. Sci. Lett., 211(3–4), 251–258, doi:10.1016/S0012-821X(03)00205-X, 2003.

Braucher, R., Del Castillo, P., Siame, L., Hidy, A. J. and Bourlés, D. L.: Determination of both exposure time and denudation rate from an in situ-produced 10Be depth profile: A mathematical proof of uniqueness. Model sensitivity and applications to natural cases, Quat. Geochronol., 4(1), 56–67, doi:10.1016/j.quageo.2008.06.001, 2009.

Braucher, R., Merchel, S., Borgomano, J. and Bourlès, D. L.: Production of cosmogenic radionuclides at great depth: A multi element approach, Earth Planet. Sci. Lett., 309(1–2), 1–9, doi:10.1016/j.epsl.2011.06.036, 2011.

Braucher, R., Bourlès, D., Merchel, S., Vidal Romani, J., Fernadez-Mosquera, D., Marti, K., Léanni, L., Chauvet, F., Arnold, M., Aumaître, G. and Keddadouche, K.: Determination of muon attenuation lengths in depth profiles from in situ produced cosmogenic nuclides, Nucl. Instruments Methods Phys. Res. Sect. B Beam Interact. with Mater. Atoms, 294, 484–490, doi:10.1016/j.nimb.2012.05.023, 2013.

Brocard, G. Y., van der Beek, P. A., Bourlès, D. L., Siame, L. L. and Mugnier, J. L.: Long-term fluvial incision rates and postglacial river relaxation time in the French Western Alps from 10Be dating of alluvial terraces with assessment of inheritance, soil development and wind ablation effects, Earth Planet. Sci. Lett., 209(1–2), 197–214, doi:10.1016/S0012-821X(03)00031-1, 2003.

Chmeleff, J., von Blanckenburg, F., Kossert, K. and Jakob, D.: Determination of the 10Be half-life by multicollector ICP-MS and liquid scintillation counting, Nucl. Instruments Methods Phys. Res. Sect. B Beam Interact. with Mater. Atoms, 268(2), 192–199, doi:10.1016/j.nimb.2009.09.012, 2010.

Cockburn, H. A. P. and Summerfield, M. A.: Geomorphological applications of cosmogenic isotope analysis, Prog. Phys. Geogr., 28(1), 1–42, doi:10.1191/0309133304pp395oa, 2004.

Desilets, D., Zreda, M. and Prabu, T.: Extended scaling factors for in situ cosmogenic nuclides: New measurements at low latitude, Earth Planet. Sci. Lett., 246(3–4), 265–276, doi:10.1016/j.epsl.2006.03.051, 2006.

Dunai, T. J.: Influence of secular variation of the geomagnetic field on production rates of in situ produced cosmogenic nuclides, Earth Planet. Sci. Lett., 193(1–2), 197–212, doi:10.1016/S0012-821X(01)00503-9, 2001.

Ebert, K., Willenbring, J., Norton, K. P., Hall, A. and Hättestrand, C.: Meteoric 10Be concentrations from saprolite and till in northern Sweden: Implications for glacial erosion and age, Quat. Geochronol., 12, 11–22, doi:10.1016/j.quageo.2012.05.005, 2012.

Frankel, K. L., Brantley, K. S., Dolan, J. F., Finkel, R. C., Klinger, R. E., Knott, J. R., Machette, M. N., Owen, L. A., Phillips, F. M., Slate, J. L. and Wernicke, B. P.: Cosmogenic 10Be and 36Cl geochronology of offset alluvial fans along the northern Death Valley fault zone: Implications for transient strain in the eastern California shear zone, J. Geophys. Res. Solid Earth, 112(6), 1–18, doi:10.1029/2006JB004350, 2007.

Granger, D. E., Lifton, N. A. and Willenbring, J. K.: A cosmic trip: 25 years of cosmogenic nuclides in geology, Bull. Geol. Soc. Am., 125(9–10), 1379–1402, doi:10.1130/B30774.1, 2013.

Hancock, G. S., Anderson, R. S., Chadwick, O. A. and Finkel, R. C.: Dating fluvial terraces with 10Be and 26Al profiles: Application to the Wind River, Wyoming, Geomorphology, 27(1–2), 41–60, doi:10.1016/S0169-555X(98)00089-0, 1999.

Heisinger, B., Lal, D., Jull, A. J. T., Kubik, P., Ivy-Ochs, S., Knie, K. and Nolte, E.: Production of selected cosmogenic radionuclides by muons: 2. Capture of negative muons, Earth Planet. Sci. Lett., 200(3–4), 357–369, doi:10.1016/S0012-821X(02)00641-6, 2002a.

Heisinger, B., Lal, D., Jull, A. J. T., Kubik, P., Ivy-Ochs, S., Neumaier, S., Knie, K., Lazarev, V. and Nolte, E.: Production of selected cosmogenic radionuclides by muons 1. Fast muons, Earth Planet. Sci. Lett., 200(3–4), 345–355, doi:10.1016/S0012-821X(02)00640-4, 2002b.

Hetzel, R., Niedermann, S., Tao, M., Kubik, P. W., Ivy-Ochs, S., Gao, B. and Strecker, M. R.: Low slip rates and long-term preservation of geomorphic features in Central Asia, Nature, 417(6887), 428–432, doi:10.1038/417428a, 2002.

Hidy, A. J., Gosse, J. C., Pederson, J. L., Mattern, J. P. and Finkel, R. C.: A geologically constrained Monte Carlo approach to modeling exposure ages from profiles of cosmogenic nuclides: An example from Lees Ferry, Arizona, Geochemistry, Geophys. Geosystems, 11(9), doi:10.1029/2010GC003084, 2010.

Korschinek, G., Bergmaier, A., Faestermann, T., Gerstmann, U. C., Knie, K., Rugel, G., Wallner, A., Dillmann, I., Dollinger, G., von Gostomski, C. L., Kossert, K., Maiti, M., Poutivtsev, M. and Remmert, A.: A new value for the half-life of 10Be by Heavy-Ion Elastic Recoil Detection and liquid scintillation counting, Nucl. Instruments Methods Phys. Res. Sect. B Beam Interact. with Mater. Atoms, 268(2), 187–191, doi:10.1016/j.nimb.2009.09.020, 2010.

Lal, D.: Cosmic ray labeling of erosion surfaces: in situ nuclide production rates and erosion models, Earth Planet. Sci. Lett., 104(2–4), 424–439, doi:10.1016/0012-821X(91)90220-C, 1991.

Lal, D. and Arnold, J. R.: Tracing quartz through the environment, Proc. Indian Acad. Sci. - Earth Planet. Sci., 94(1), 1–5, doi:10.1007/BF02863403, 1985.

Laloy, E., Beerten, K., Vanacker, V., Christl, M., Rogiers, B. and Wouters, L.: Bayesian inversion of a CRN depth profile to infer Quaternary erosion of the northwestern Campine Plateau (NE Belgium), Earth Surf. Dyn., 5(3), 331–345, doi:10.5194/esurf-5-331-2017, 2017.

Lifton, N. A., Bieber, J. W., Clem, J. M., Duldig, M. L., Evenson, P., Humble, J. E. and Pyle, R.: Addressing solar modulation and long-term uncertainties in scaling secondary cosmic rays for in situ cosmogenic nuclide applications, Earth Planet. Sci. Lett., 239(1–2), 140–161, doi:10.1016/j.epsl.2005.07.001, 2005.

Marrero, S. M., Phillips, F. M., Borchers, B., Lifton, N., Aumer, R. and Balco, G.: Cosmogenic nuclide systematics and the CRONUScalc program, Quat. Geochronol., 31, 160–187, doi:10.1016/j.quageo.2015.09.005, 2016.

Matsushi, Y., Wakasa, S., Matsuzaki, H. and Matsukura, Y.: Long-term denudation rates of actively uplifting hillcrests in the Boso Peninsula, Japan, estimated from depth profiling of in situ-produced cosmogenic 10Be and 26Al, Geomorphology, doi:10.1016/j.geomorph.2006.05.009, 2006.

Nishiizumi, K., Imamura,Mercader, J., Gosse, J. C., Bennett, T., Hidy, A. J. and Rood, D. H.: Cosmogenic nuclide age constraints on Middle Stone Age lithics from Niassa, Mozambique, Quat. Sci. Rev., 47, 116–130, doi:10.1016/j.quascirev.2012.05.018, 2012.

M., Caffee, M. W., Southon, J. R., Finkel, R. C. and McAninch, J.: Absolute calibration of 10Be AMS standards, Nucl. Instruments Methods Phys. Res. Sect. B Beam Interact. with Mater. Atoms, 258(2), 403–413, doi:10.1016/j.nimb.2007.01.297, 2007.

Repka, J. L., Anderson, R. S. and Finkel, R. C.: Cosmogenic dating of fluvial terraces, Fremont River, Utah, Earth Planet. Sci. Lett., 152(1–4), 59–73, doi:10.1016/s0012-821x(97)00149-0, 1997.

Riihimaki, C. A., Anderson, R. S., Safran, E. B., Dethier, D. P., Finkel, R. C. and Bierman, P. R.: Longevity and progressive abandonment of the Rocky Flats surface, Front Range, Colorado, Geomorphology, 78(3–4), 265–278, doi:10.1016/j.geomorph.2006.01.035, 2006.

Rixhon, G., Briant, R. M., Cordier, S., Duval, M., Jones, A. and Scholz, D.: Revealing the pace of river landscape evolution during the Quaternary: recent developments in numerical dating methods, Quat. Sci. Rev., 166, 91–113, doi:10.1016/j.quascirev.2016.08.016, 2017.

Ruszkiczay-Rüdiger, Z., Braucher, R., Novothny, Á., Csillag, G., Fodor, L., Molnár, G. and Madarász, B.: Tectonic and climatic control on terrace formation: Coupling in situ produced 10Be depth profiles and luminescence approach, Danube River, Hungary, Central Europe, Quat. Sci. Rev., 131, 127–147, doi:10.1016/j.quascirev.2015.10.041, 2016.

Stone, J. O.: Air pressure and cosmogenic isotope production, J. Geophys. Res. Solid Earth, 105(B10), 23753–23759, doi:10.1029/2000JB900181, 2000.

Wang, Y., Oskin, M. E., Zhang, H., Li, Y., Hu, X. and Lei, J.: Deducing Crustal-Scale Reverse-Fault Geometry and Slip Distribution From Folded River Terraces, Qilian Shan, China, Tectonics, 39(1), doi:10.1029/2019TC005901, 2020.